HHS Public Access

Author manuscript

Dev Neurobiol. Author manuscript; available in PMC 2019 December 19.

Intraspinal serotonergic signaling suppresses locomotor activity in larval zebrafish

Jacob E. Montgomery[*,1], **Sarah Wahlstrom-Helgren**[1], **Timothy D. Wiggin**[1], **Brittany M. Corwin**[1], **Christina Lillesaar**[2], and **Mark A. Masino**[1]

[1]University of Minnesota, Department of Neuroscience, Minneapolis, MN

[2]University of Würzburg, Department of Physiological Chemistry, Biocenter, Würzburg, Germany

Abstract

Serotonin (5HT) is a modulator of many vital processes in the spinal cord (SC), such as production of locomotion. In the larval zebrafish, intraspinal serotonergic neurons (ISNs) are a source of spinal 5HT that, despite the availability of numerous genetic and optical tools, has not yet been directly shown to affect the spinal locomotor network. In order to better understand the functions of ISNs, we used a combination of strategies to investigate ISN development, morphology, and function. ISNs were optically isolated from one another by photoconverting Kaede fluorescent protein in individual cells, permitting morphometric analysis as they developed *in vivo*. ISN neurite lengths and projection distances exhibited the greatest amount of change between 3 and 4 days post-fertilization (dpf) and appeared to stabilize by 5 dpf. Overall ISN innervation patterns were similar between cells and between SC regions. ISNs possessed rostrally-extending neurites resembling dendrites and a caudally-extending neurite resembling an axon, which terminated with an enlarged growth cone-like structure. Interestingly, these enlargements remained even after neurite extension had ceased. Functionally, application of exogenous 5HT reduced spinally-produced motor nerve bursting. A selective 5HT reuptake inhibitor and ISN activation with channelrhodopsin each produced similar effects to 5HT, indicating that spinally-intrinsic 5HT originating from the ISNs has an inhibitory effect on the spinal locomotor network. Taken together this suggests that the ISNs are morphologically mature by 5 dpf and supports their involvement in modulating the activity of the spinal locomotor network.

Keywords

morphology; optogenetic; serotonin; spinal cord; zebrafish

Introduction

Serotonin (5HT) is found nearly ubiquitously in living organisms and serves a wide variety of functions both between, and within species. 5HT functions as a neurotransmitter in the nervous system, playing important roles in processes including digestion, circadian rhythms,

[*]Correspondence sent to: Jacob E. Montgomery, Department of Neuroscience, University of Minnesota, 3-145 Jackson Hall, 321 Church Street, Minneapolis, MN 55455, mont0306@umn.edu, Phone: 612-625-4412, Fax: 612-626-5009.

Conflict of Interest Statement: The authors have no conflicts of interest to report.

learning and memory, sensation, and behavior (Berger et al., 2009). Serotonergic signaling is accomplished in a variety of ways; through any of the 14 G protein-coupled or ionotropic 5HT receptor (5HTR) subtypes identified in mammals (Hoyer et al., 1994; Barnes and Sharp, 1999) and through transmission at synapses or extrasynaptically through volume transmission (Ridet et al., 1993; Bunin and Wightman, 1999; Fuxe et al., 2007). Therefore, investigations of the 5HT system require a systematic approach to isolate its mechanisms of action.

Consistent with its pervasiveness within the nervous system, 5HT affects the activity of many neural networks within the spinal cord (SC), including the spinal locomotor network (Schmidt and Jordan, 2000). 5HT is sufficient to elicit fictive locomotor activity in spinally-transected rabbits (Viala and Buser, 1974) and in isolated neonatal rat and mouse SCs (Cazalets et al., 1992; Nishimaru et al., 2000). Modulation of spinal motor neurons and interneurons by 5HT is a shared phenomenon among all vertebrate classes (Harris-Warrick and Cohen, 1985; Rossignol and Dubuc, 1994; Sillar et al., 1998; Schmidt and Jordan, 2000). Spinal 5HT also promotes neuronal regeneration, network reorganization, and recovery of locomotor function following SC injury, which can be manipulated through pharmacological enhancement of 5HT signaling or transplantation of serotonergic neurons caudal to the site of injury (Ghosh and Pearse, 2014; Barreiro-Iglesias et al., 2015). The prevalence of 5HT in the SC, combined with its potential therapeutic effects, has helped to drive decades of research into the spinal 5HT system.

The raphe nuclei innervate the SC from the hindbrain, providing the mammalian SC with the majority of its 5HT (Dahlström and Fuxe, 1964; Steinbusch, 1981). The observation that 5HT was not entirely eliminated from the SC after complete, chronic spinal transection from the brain led to the inferred existence of spinally-intrinsic serotonergic neurons (Carlsson et al., 1963; Andén et al., 1964; Shibuya and Anderson, 1968; Clineschmidt et al., 1971). Subsequent development of immunohistochemical labeling techniques (Steinbusch et al., 1978) assisted both in confirming and characterizing intraspinal serotonergic neurons (ISNs) in a wide variety of vertebrates, including teleost and non-teleost fishes (Parent and Northcutt, 1982; Ritchie and Leonard, 1982; Harris-Warrick et al., 1985; Van Dongen et al., 1985b; Onstott and Elde, 1986; Van Raamsdonk et al., 1996; McLean and Fetcho, 2004a), chicks (Sako et al., 1986; Wallace et al., 1986), murids (Newton et al., 1986; Ballion et al., 2002), and monkeys (Lamotte et al., 1982). Robust innervation of the SC with descending serotonergic fibers from the raphe is well-conserved; however, both the number and location of ISNs are variable between species (Schmidt and Jordan, 2000; Lillesaar, 2011). Mammalian ISNs tend to be restricted to certain levels of the SC (Lamotte et al., 1982; Newton and Hamill, 1988; Ballion et al., 2002), whereas non-mammalian ISNs are more evenly-distributed along the rostrocaudal axis (Ritchie and Leonard, 1982; Harris-Warrick et al., 1985; McLean and Fetcho, 2004a).

The proposed functions of ISNs are related to their number and location, as well as the regions of the SC that they innervate. For example, rats have very few, dorsally-located ISNs, therefore these ISNs are hypothesized to play an autonomic or nociceptive function (Newton and Hamill, 1988). In contrast, fish have considerably more numerous ISNs that are typically located in the ventral SC, near the locomotor-generating circuitry that they are

believed to modulate (Harris-Warrick et al., 1985; Van Dongen et al., 1985a; Van Raamsdonk et al., 1996; McLean and Fetcho, 2004b). Consistent with this hypothesis, NMDA-induced locomotor activity is modulated by selective 5HT reuptake inhibitors (SSRIs) in isolated lamprey SCs (Christenson et al., 1989; Zhang and Grillner, 2000), demonstrating that 5HT produced by spinally-intrinsic sources modulates the spinal locomotor network.

The combination of transparency and genetic tractability of the larval zebrafish permits *in vivo* visualization and perturbation of neurons in an intact vertebrate system, making them especially amenable to the study of neural networks and their development. In developing embryonic zebrafish, 5HT-immunoreactive (5HT-ir) Kolmer-Agduhr neurons in the ventral SC express the 5HT-synthesizing enzyme *tryptophan hydroxylase 1a* (*tph1a*) between approximately 1 and 2.5 days post fertilization (dpf(Bellipanni et al., 2002; Montgomery et al., 2016). The Kolmer-Agduhr neurons gradually lose *tph1a* expression and 5HT-immunoreactivity as a separate population of ISNs and descending raphe projection fibers complete innervation of the SC at approximately 4 dpf (McLean and Fetcho, 2004a; Montgomery et al., 2016), coinciding with development of the mature beat-and-glide swimming pattern in larval-stage zebrafish (Buss and Drapeau, 2001). This later-appearing population of ISNs expresses *tryptophan hydroxylase 2* (*tph2*) instead of *tph1a* and persists until at least 10 dpf (Montgomery et al., 2016). 5HT-ir neurons have also been confirmed in the ventral SC of adult zebrafish (Van Raamsdonk et al., 1996; Kuscha et al., 2011; Barreiro-Iglesias et al., 2015), although *tph* gene expression in these cells has not been characterized.

Larval zebrafish ISN somas are evenly-distributed along the rostrocaudal axis of the SC, ovoid, of a consistent size, and ventrally located (Brustein et al., 2003; McLean and Fetcho, 2004a), slightly lateral to the ventral-most Kolmer-Agduhr neurons (Montgomery et al., 2016). Immunohistochemistry and stochastic labeling with green fluorescent protein (GFP) have shown that ISNs possess single processes that extend dorsolaterally into the motor column and split into putative dendritic processes and a caudal projection resembling an axon (Brustein et al., 2003; McLean and Fetcho, 2004a; McLean and Fetcho, 2004b). The caudal projections appeared to terminate with a growth cone 1–2 body segments from the soma, although processes from individual ISNs were difficult to discriminate from one another and from projections originating in the brain (McLean and Fetcho, 2004a).

The recent identification of ISN-specific zebrafish *pet1* and *tph2* promoters (Lillesaar et al., 2009; Yokogawa et al., 2012), combined with the development of photoconvertible fluorescent proteins, facilitates *in vivo* optical isolation and investigation of individual ISNs and their projection patterns. We used these tools to quantify ISN localization, development, and morphometry, expanding upon previous immunohistochemistry-based descriptions. We also used pharmacologic and optogenetic tools to perturb the spinal 5HT system to enhance 5HT signaling in the SC, which produced a decrease in spinally-generated locomotor bursting activity. Together, this supports a role for the ISNs in modulating activity of the spinal locomotor network.

Materials and Methods

Zebrafish Lines and Maintenance

Adult zebrafish were maintained at the University of Minnesota Zebrafish Core Facility using standard practices (Tye et al., 2015). Embryos and larvae were raised at 28.5°C with a 14-h light:10-h dark cycle in embryo water containing 60 μg/mL Instant Ocean (Blacksburg, VA) Sea Salt. All experimental protocols were approved by the University of Minnesota Institutional Animal Care and Use Committee. Animals used in the study included wild-type zebrafish (Segrest Farms, Gibsonton, FL) and the previously described *Tg(pet1:EGFP)*^{ne0214} (Lillesaar et al., 2009) and *Tg(UAS:Kaede)*^{s1999t} (Scott et al., 2007) transgenic lines. The *Tg(pet1:gal4-p2A-EGFP)*^{gy1} line containing the *−3.2 kb pet1* promoter (Lillesaar et al., 2009) upstream of *Gal4VP16* (Köster and Fraser, 2001) fused to *EGFP* with a *P2A* self-cleaving peptide (Holst et al., 2006) was published earlier as *Tg(fev:GAL4-GFP)*^{gy1} (Xing et al., 2015).

To generate the *Tg(UAS:ChR2(H134R)-mCherry)* line, *ChR2(H134R)-mCherry* was subcloned from the *pcDNA3.1/hChR2(H134R)-mCherry* plasmid (Addgene plasmid #20938; Zhang et al., 2007) into the *pME-MCS* Gateway middle entry clone (Kwan et al., 2007) using *KpnI* and *NotI*. The resulting plasmid was used in an LR Gateway reaction with the *p5E-UAS* 5′ entry clone, *p3E-polyA* 3′ entry clone, and the *pDestTol2pA2* destination vector (Kwan et al., 2007) to make the final *pDestTol2pA2-UAS-ChR2(H134R)-mCherry* expression construct. Capped *Tol2 transposase* mRNA was *in vitro* transcribed from the *PCS2FA-transposase* plasmid (Kwan et al., 2007) using the SP6 mMessage mMachine kit (Ambion, Foster City, CA). *Tol2 transposase* mRNA was co-injected with the *pDestTol2pA2-UAS-ChR2(H134R)-mCherry* expression construct (25 ng/μl each) into 1–4 cell-stage wild-type zebrafish embryos as described (Kawakami, 2004).

Immunohistochemistry

For whole-mount larval immunohistochemistry, 5 dpf larvae were anesthetized with a lethal dose of 0.2% Tricaine-S (Western Chemical, Ferndale, WA), fixed in 4% paraformaldehyde, digested with Proteinase K (40 μg/mL), incubated with primary and secondary antibodies, and embedded in low melting-point agarose as described previously (Montgomery et al., 2016). Antibodies used included rabbit polyclonal anti-5HT primary (S5545, 1:400; Sigma-Aldrich, St. Louis, MO), mouse monoclonal anti-synaptic vesicle protein glycoprotein 2A primary (SV2, 1:20; Developmental Studies Hybridoma Bank, Iowa City, IA), and Alexa Fluor 633 goat anti-rabbit secondary antibody (A-21071, 1:500; Thermo Fisher Scientific Inc., Waltham, MA). Anti-SV2 was deposited to the Developmental Studies Hybridoma Bank by Buckley, KM (Buckley and Kelly, 1985).

For immunohistochemistry in adult SC sections, *Tg(pet1:EGFP)*^{ne0214} zebrafish (6 months post-fertilization) were anesthetized and dissected in cold 0.2% Tricaine-S. SC specimens were removed from the region of the SC corresponding to the ventral body cavity (between vertebrae 7 and 15) and fixed in 4% paraformaldehyde/1× PBS 4°C overnight. Specimens were washed and cryoprotected in 5% sucrose/1× PBS at 4°C overnight, then were oriented for sectioning and embedded in 1.5% agarose/5% sucrose/1× PBS. Samples were finally

infiltrated 4°C overnight each with, in order: 30% sucrose/1× PBS, 30% sucrose/1× PBS:O.C.T. Compound (1:1; Sakura Finetek USA Inc., Torrance, CA), and 100% O.C.T. Compound. Transverse and sagittal frozen sections (30 μm) were collected on slides, dried for 2 h at 50°C, and stored at −80°C. For immunolabeling, slides were warmed for 20 min at 50°C, rehydrated in 1× PBS for 20 min, incubated in blocking solution (2.5% bovine serum albumin, 0.3% Triton X-100, and 1% DMSO in 1× PBS) for 1 h, and labeled with rabbit polyclonal anti-5HT primary antibodies (1:400 in blocking solution) 4°C overnight. Sections were washed 3 times with 0.05% Tween-20/1× PBS, incubated with Alexa Fluor 633 goat anti-rabbit secondary antibodies (1:500 in blocking solution) 1 h at room temperature, and washed 3 more times with 0.05% Tween-20/1× PBS. To reduce lipofuscin-like autofluorescence in vasculature, sections were briefly rinsed with distilled water, incubated in 10 mM Copper(II) sulfate pentahydrate in 50 mM ammonium acetate (pH 5.0) for 1 h at room temperature, rinsed again with distilled water, and rinsed with 1× PBS as described (Schnell et al., 1999). Labeled slides were mounted with coverslips using Vectashield Antifade Mounting Medium (Vector Laboratories, Inc., Burlingame, CA).

Confocal image acquisition

Live zebrafish larvae were anesthetized with 0.02% Tricaine-S, embedded laterally or dorsally in 1.5% low melting-point agarose, and covered with 0.02% Tricaine-S. Confocal images of live and fixed whole-mount larvae and adult SC sections were acquired with an Olympus FluoView FV1000 confocal microscope (Center Valley, PA). Dual-wavelength differential fluorescence correction was used to reduce autofluorescence in labeled channels of adult SC sections (Steinkamp and Stewart, 1986; Billinton and Knight, 2001). Image processing and enhancements were applied to entire panels using FIJI (Schindelin et al., 2012) and Photoshop CS5 (Adobe Systems, San Jose, CA).

ISN distribution

To quantify and plot the position of ISN cell somas within the SC, live 3, 5, 7, and 10 dpf T*g(pet1:EGFP)*^{ne0214} larvae (n=5, 5, 7, and 6, respectively) were embedded laterally in 1.5% low melting-point agarose and overlapping confocal z-stacks were collected along the entire rostrocaudal SC axis using a 40× water immersion objective. Z-stacks (9 stacks per larva) were merged with the Grid/Collection Stitching FIJI plugin (Preibisch et al., 2009) to create a single composite stack. The Cell Counter FIJI plugin was used to place counters along the lateral, dorsal, and ventral SC boundaries and centered on EGFP-positive somas. Cell Counter measurements were used to plot the position of all ISN somas in Matlab (Mathworks, Natick, MA) and Microsoft Excel (Redmond, WA). Body segment numbers one and two (rostral to the hindbrain/SC boundary) were excluded to restrict analysis to only the SC. Rostrocaudal positions were plotted as distance from the segment 2/3 boundary, while dorsoventral and lateral positions were plotted as proportion of SC height and width, respectively to account for the narrowing of the SC along the rostrocaudal axis. SC half-widths were calculated to approximate the lateral SC boundaries in lateral soma position plots to correct for body curvature resulting from agarose embedding.

Kaede photoconversion and morphometric analysis

Tg(pet1:gal4-p2A-EGFP)^{gy1};*Tg(UAS:Kaede)*^{s1999t} larvae were raised in the dark to prevent photoconversion of Kaede fluorescent protein (Ando et al., 2002). Live larvae were embedded laterally in 1.5% low melting-point agarose. Using the Olympus FluoView FV1000 photobleaching tool, a region of interest was drawn around individual Kaede-expressing ISN somas, and somas were continuously exposed to low intensity (8%) UV (405 nm wavelength) light for 30–60 s with a 60× water immersion objective. Confocal Z-stacks were collected across the entire width of the SC 5–10 min after UV light exposure in 3–10 dpf larvae. For single timepoint morphometric analysis, ISNs were imaged only once. For longitudinal study of ISN morphological development, larvae were unembedded after photoconversion and imaging, returned to embryo water in dark conditions, and photoconverted ISNs were reimaged the following day, repeated up to six times. If red Kaede fluorescence was low during ISN reimaging, additional UV light was applied to the cell to photoconvert more Kaede protein.

Morphometric measurements of photoconverted ISNs were made in FIJI. Rostral, caudal, and dorsal projection distances were measured using a straight horizontal or vertical line originating from the center of the soma to the furthest projection terminal from the soma in each direction. Lateral projection distances were measured in 3D projections rotated 90° along the rostrocaudal axis. All processes of individual photoconverted ISNs were traced and skeletonized in confocal Z-stacks with the Simple Neurite Tracer FIJI plugin (Longair et al., 2011) to identify and measure the longest rostrally and caudally projecting neurites. Traced paths were filled out with Simple Neurite Tracer and thresholded. Three-dimensional Sholl analysis (Ferreira et al., 2014) of thresholded Z-stacks was performed in FIJI to calculate the number of intersections at radii increasing in increments of 1 μm originating from the center of the cell soma. Sholl analysis included quantification of critical value (maximum number of intersections), critical radius (radius containing the maximum number of intersections), and maximum projection distance/enclosing radius for each photoconverted cell. Temporal changes to ISN morphometric measurements were expressed as percent change in the measures from one day to the next.

Peripheral nerve recordings and analysis

Larvae (5–7 dpf) were anesthetized with 0.02% Tricaine-S in extracellular saline (in mM: 134 NaCl, 2.9 KCl, 1.2 $MgCl_2$, 2.1 $CaCl_2$, 10 HEPES), pH 7.8, mOsm: 290–300 (adjusted with sucrose). Larvae were prepared for peripheral motor nerve recording by pinning them laterally to a Sylgard-lined dissecting dish, skinning, and paralyzing for 10 min with 250 μM α-bungarotoxin (Tocris, Bristol, UK) as described previously (Masino and Fetcho, 2005). An FA-10 Feather S razor blade (Ted Pella, Redding, CA) was used to sever the SC and dorsal body trunk at segment 3–4. Preparations were placed on an Olympus BX51 WI microscope (Center Valley, PA) and constantly perfused with extracellular saline at room temperature. N-Methyl-D-aspartic acid (NMDA, 50–75 μM; Sigma-Aldrich) was added to the perfusate to induce fictive locomotor activity in the spinally-transected preparations. Glass suction electrodes filled with extracellular saline were attached to motor nerves in the intermyotomal clefts and voltage was recorded with a Multiclamp 700B amplifier and

Digidata 1440A digitizer using pClamp 10 software (Molecular Devices, Sunnyvale, CA) as described previously (Wiggin et al., 2012).

Zebrafish locomotion consists of discrete swimming episodes that are made up of motor bursting corresponding to the contraction of one side of the body (Masino and Fetcho, 2005). Bursting activity and its properties in peripheral nerve voltage recordings were analyzed in Matlab (Wiggin et al., 2012). Episodic organization (EO) scores were calculated to quantify the organization of fictive locomotor bursting into episodes by testing the bimodality of inter-burst periods as previously described (Wiggin et al., 2012). A bimodal distribution of inter-burst periods indicated that bursts consisted of those within an episode and those that spanned two episodes, resulting in a high EO score. A non-bimodal distribution indicated that bursting occurred that was not grouped into episodes, resulting in a lower EO score. Values were expressed as a percentage of the baseline when comparing fictive swimming properties between preparations to account for individual Baseline differences.

Pharmacology

Wild-type larvae were perfused with extracellular saline with 50–75 μM NMDA for 20–30 min prior to voltage recordings. NMDA-induced baseline nerve activity was recorded for 10 min, 5HT (Sigma-Aldrich; n=8) or citalopram hydrobromide (Sigma-Aldrich; n=6) was added to the perfusate for 15 min, and then a wash out with saline containing only NMDA was recorded for 30 min. The final 2 min of each recording condition was used for analysis. 5HT (1 μM) and citalopram (5 μM) concentrations were selected after dose-response experiments found that they consistently elicited locomotor activity changes without abolishing episodic swimming activity (not shown).

Light Stimulation

Spinally-transected *Tg(pet1:gal4-p2A-EGFP)*^{gy1};*Tg(UAS:ChR2(H134R)-mCherry)* larvae (n=13) were prepared for peripheral motor nerve recordings and perfused with NMDA-containing extracellular saline. Extracellular peripheral nerve recordings were initiated after 15–30 min of NMDA bath perfusion. TTL pulses from an A-M Systems (Sequim, WA) Model 2100 Isolated Pulse Stimulator were used to activate an E-Cite Series 120 Q lamp (Excelitas Technologies, Waltham, MA). Light was delivered through a FITC filter set (number 41001, Chroma Technology, Bellows Falls, VT) and 20× water immersion objective on an Olympus BX51 WI microscope. TTL trains were delivered for 30 s at 5 Hz with 50 ms pulse durations. Fictive locomotor activity was analyzed as described above on the 30 s immediately preceding, during, and following light delivery. In control trials, 11 of the experimental *Tg(pet1:gal4-p2A-EGFP)*^{gy1};*Tg(UAS:ChR2(H134R)-mCherry)* larvae were also exposed to trains of red light (Supporting Information Fig. S1) through a Cy5 filter set (number 41008, Chroma Technology). To control for potential effects of blue light exposure, *Tg(pet1:gal4-p2A-EGFP)*^{gy1} clutchmates that did not express *ChR2* (n=4) were exposed to trains of blue light as described above (Supporting Information Fig. S2). Since *UAS:ChR2(H134R)-mCherry* expression was variegated, the number of cells displaying mCherry fluorescence was quantified in the skinned region of each preparation.

Statistical Analysis

Mean data is expressed as mean with SD and error bars represent one SD from the mean. Student's t-tests and one-way and two-way ANOVAs were used to identify significant effects when appropriate. ANOVAs that showed a significant effect were followed by Bonferroni-corrected post-hoc t-tests for morphometric data and Tukey's HSD post-hoc tests for electrophysiology data. Significance was tested at an α value of 0.05.

Results

Location and distribution

The *Tg(pet1:EGFP)*^{ne0214} line, which specifically labels serotonergic neurons and descending raphe fibers in the SCs of 4 through 10 dpf larvae (Lillesaar et al., 2009; Montgomery et al., 2016), was used to examine the ISNs at 5 dpf. Live larvae were embedded in agarose and confocal Z-stacks were collected from the midbody region (centered on body segment 15) of the SC. A Z-projected lateral view of the midbody region revealed fluorescently labeled somas in the ventral SC and fibers in the ventral and dorsal SC (Fig. 1A). A 90-degree rotation of the same Z-stack along the dorsoventral axis showed that processes were concentrated at the lateral edges of the SC, although ISN processes could not be distinguished from those originating in the hindbrain (Fig. 1A′). A Z-stack collected from a dorsal perspective indicated that the ISN somas were slightly lateral to the midline and fluorescently labeled fibers only occasionally crossed the midline (Fig. 1B). Z projections of only the ventral SC (Fig. 1B′) confirmed that the ISNs projected laterally, and that some cells possessed two lateral projections originating from the soma (arrowheads).

ISN soma location and distribution were examined in composite confocal Z-stacks of entire 5 dpf *Tg(pet1:EGFP)*^{ne0214} SCs. To visualize the positions of all ISNs in a single SC, soma positions from one larva were plotted along the rostrocaudal, mediolateral, and dorsoventral axes (Fig. 1C and D). Somas were distributed along the entire rostrocaudal axis of the SC and were located bilaterally in the ventral SC. Next, ISN soma positions in multiple 5 dpf SCs (n=5) were normalized and divided into 20 bins based on distance from the hindbrain/SC junction (defined as the intersection of body segments 2 and 3; Fig. 1E), the midline (Fig. 1F), and the SC floor (Fig. 1G). Analysis of the entire rostrocaudal axis of the SC revealed an effect of bin number on the number of cells in each bin (single factor ANOVA; $F=3.92$; $p<0.001$), while analysis excluding the caudal-most bin did not show an effect of bin number on cell number (single factor ANOVA; $F=1.07$; $p>0.05$). This demonstrated that the ISNs were distributed evenly along the rostrocaudal axis, excepting the caudal-most 5% of the SC, which contained 9.4 cells compared to the other bins that each contained between 3.0 and 5.2 cells (Fig. 1E; mean cells per bin (bins 1–19) = 4.52, SD 1.28). The mean distance of all ISN somas from the midline was 24.3% (SD 12.2) of the SC half-width (Fig. 1F) and somas were restricted to the ventral-most 8.0% (SD 5.2) of the SC (Fig. 1G). The distribution of ISNs was similar at 3, 5, 7, and 10 dpf, although the higher number of ISNs found in the caudal-most SC was not observed in 3 dpf larvae (not shown). Furthermore, the mean number of ISNs in the SC (3 dpf: 74.6, SD 14.9, n=5; 5 dpf: 90.4, SD 10.0, n=5; 7 dpf: 84.3, SD 10.5, n=7; 10 dpf: 80.3, SD 3.3, n=6) was not significantly different between the same ages (single factor ANOVA; $F=2.13$; $p>0.05$).

Embryonic zebrafish possess a population of 5HT-containing spinal neurons that express *tph1a* (Bellipanni et al., 2002), while larval stage ISNs express *tph2* and *pet1*, and can be identified by EGFP expression in the *Tg(pet1:EGFP)*^{ne0214} line (Montgomery et al., 2016). Although 5HT-ir ISNs have been reported in the ventral adult zebrafish SC (Van Raamsdonk et al., 1996; Barreiro-Iglesias et al., 2015), the *tph* gene expressed by these cells is not known. Examination of sagittal and transverse frozen sections of adult *Tg(pet1:EGFP)*^{ne0214} SCs (n=6) verified that *pet1:EGFP*-expressing cells were ventrally-located and colabeled with 5HT antibodies (red; Fig. 1H and I; 110 of 111 EGFP+ cells) and that 5HT-ir cells expressed *pet1:EGFP* (110 of 110 5HT-ir cells). *Pet1* specifies *tph2*-expressing neurons (Lillesaar et al., 2007; Liu et al., 2010; Montgomery et al., 2016), therefore adult zebrafish ISNs are putatively the same population of *tph2*-expressing ISNs that are present in larvae.

Morphological changes

In zebrafish larvae, differentiation of the persistent population of *pet1*-expressing ISNs primarily occurs between 2.5 and 3 dpf (Montgomery et al., 2016). Spinal 5HT innervation is established by 4 dpf and maintained through 10 dpf (McLean and Fetcho, 2004a), although developmental changes to the projections of individual ISNs have not been studied. We confirmed ISN-specific expression of *Gal4-p2A-EGFP* in the *Tg(pet1:Gal4-p2A-EGFP)*^{gy1} line by labeling 5 dpf larvae with 5HT antibodies (Fig. 2A). Quantification of fluorescently-labeled cells in the midbody region of the SC revealed both that EGFP-expressing cells were 5HT-ir (151 of 153) and that all 5HT-ir cells expressed EGFP (n=12 larvae). Next, the *Tg(pet1:Gal4-p2A-EGFP)*^{gy1} and *Tg(UAS:Kaede)*^{s1999t} (Scott et al., 2007) lines were crossed to drive expression of the photoconvertible Kaede fluorescent protein (Ando et al., 2002) in progeny under control of the ISN-specific *pet1* promoter. Green fluorescence was observed in ventrally-located somas and in rostrocaudally projecting fibers in both the dorsal and ventral SC (Fig. 2B). To optically isolate ISNs, Kaede was photoconverted to its red form in single cells, revealing individual cell somas and processes, which were restricted to the ventral SC (Fig. 2B′ and B″). Finally, photoconverted ISN somas and processes were traced, filled, and thresholded in confocal Z-stacks for morphometric analysis (Fig. 2B‴).

Individual Kaede-expressing ISNs were photoconverted between 3 and 5 dpf. Confocal images were acquired immediately after photoconversion and at one day increments following photoconversion to track the morphological changes undergone by ISNs during larval development. Morphometric properties of photoconverted cells were measured at 3–7 dpf and at 10 dpf (Fig. 3A). Projection distances (rostrocaudal, rostral, caudal, dorsal, and lateral; Fig. 3B, ①–⑤, respectively) were measured in confocal Z-stacks from the center of each soma. Three-dimensional Sholl analysis originating from the center of cell somas in thresholded Z-stacks identified maximum projection distances (Fig. 3B, ⑥), critical values (maximum number of intersections), and critical radii (radius at which the critical value occurs; Fig. 3B, ⑦). Finally, the lengths of the longest rostrally and caudally projecting neurites were measured (Fig. 3B, ⑧ and ⑨, respectively). The change to each measure was expressed as percent change from one day to the next (Table 1). To illustrate morphometric changes over time, the percent change for individual ISNs (gray dots) and mean percent change (horizontal black bars) were plotted for a subset of the metrics (total rostrocaudal

projection distance, dorsal projection distance, maximum projection distance, and critical value) over each timespan (Fig. 3C). The largest mean percent change for each metric occurred between 3 and 4 dpf and none of the metrics changed significantly after 5 dpf (Table 1). Thus, ISN innervation patterns as a whole exhibited the greatest change before 4 dpf and stabilized after 5 dpf.

Morphological features

Zebrafish ISNs have been qualitatively described as having dendrites that project dorsally and laterally with a single, descending axon that projects 1–2 body segments caudally (Brustein et al., 2003; McLean and Fetcho, 2004a). To more precisely distinguish and quantify ISN morphometry, individual Kaede-expressing ISNs were optically isolated. Confocal Z-stacks of optically isolated ISNs were acquired from live 5–7 dpf larvae (Fig. 4, n=46), since no significant morphometric changes were found after 5 dpf (Fig. 3 and Table 1). Three-dimensional projections of the ISNs were rotated along the rostrocaudal and dorsoventral axes to produce images from the lateral, dorsal, and transverse perspectives (Fig. 4A). The majority of cells analyzed (30 out of 46) were unipolar, extending a single neurite that diverged into rostral and caudal projections, while the others appeared to be bipolar (16 out of 46), with one caudally-projecting and one rostrally-projecting neurite originating from the soma (Fig. 4A, arrows). Presumptive dendritic processes branched dorsal and rostral to the soma, and cells had a single caudal projection that resembled an axon. Putative axon terminals consisted of an enlarged, and occasionally bifurcated, structure (Fig. 4A, arrowheads).

In agreement with these qualitative observations, averaged Sholl data (Fig. 4B) demonstrated that the greatest number of intersections (critical value; 5.63, SD 1.79) occurred near the soma (at 16 μm radius), corresponding to the location of dendritic branching. There were fewer intersections further from the soma (1.32, SD 0.56 and 1.30, SD 0.48 intersections at radii of 50 and 100 μm, respectively), which was consistent with the extension of a single caudally-projecting process. The Sholl plot in Fig. 4B contained only one cell that projected beyond 128 μm. Projection distances, neurite lengths, and critical radii were quantified for each ISN (Fig. 4C). Both caudal projection distance (78.8 μm, SD 25.5) and neurite length (105.8 μm, SD 29.0) were significantly greater than rostral projection distance (36.5 μm, SD 13.8) and length (57.0 μm, SD 16.2; paired t-tests; both $p<0.001$). The mean rostrocaudal length of body segments containing each of the photoconverted ISN somas was 87.4 μm (SD 7.2) and the mean ISN rostrocaudal projection distance was 115.3 μm (SD 27.8), thus each ISN spanned approximately two body segments.

To verify the axonal identity of the caudal process and terminal structure, Kaede was photoconverted in 5 dpf larvae, which were processed with antibodies to SV2 (Fig. 5). Since expression of *UAS:Kaede* was variegated, photoconverted Kaede fluorescence could be used to identify ISNs and their caudal projections (Fig. 5A). Magnified single plane images (region indicated by the dashed box in panel A) of Kaede fluorescence (pseudocolored green) and SV2 antibody labeling (pseudocolored red) at the caudal terminals revealed punctate labeling of SV2 within the terminal structures (Fig. 5B-B″). This confirmed that

the caudal ISN projections and their large terminal structures were axons and axon terminals, respectively.

Spinal 5HT and locomotor output

Although 5HT is believed to play many functions in the production and modulation of locomotion, its aggregate effect on locomotor activity produced in the zebrafish SC is not known. To test the effects of 5HT on the output of the spinal locomotor circuitry, we severed all fibers descending to the SC from the brain, including the serotonergic raphe fibers, by spinally-transecting larvae (5–7 dpf) caudal to the hindbrain. Preparations were paralyzed, fictive locomotion was induced through bath perfusion of NMDA (McDearmid and Drapeau, 2006; Lambert et al., 2012; Wiggin et al., 2012), and peripheral motor nerve activity was recorded with extracellular suction electrodes (Masino and Fetcho, 2005). Fictive locomotor output consists of bursts of activity that correspond to muscle contraction on one side of the body. These bursts normally alternate laterally, giving rise to the side-to-side flexions that make up swimming. Three or more temporally-grouped unilateral bursts were defined as swimming episodes corresponding to the active periods of swimming in free-swimming larvae (Masino and Fetcho, 2005). Motor nerve activity was recorded in NMDA for 30 min (Baseline), 5HT was added to the NMDA-perfusate for 15 min, and this was followed by a 30 min washout with 5HT-free NMDA (Washout; Fig. 6).

The number of fictive locomotor bursts and their organization into discrete episodes of swimming (EO score) were calculated as a percent of the baseline to normalize Baseline variability between preparations (Fig. 6C and D). Treatment condition caused a significant effect on NMDA-driven motor nerve bursting (single factor ANOVA, $F=6.93$, $p<0.005$) but not EO score (single factor ANOVA, $F=0.82$, $p>0.05$). There were fewer bursts during 5HT treatment (73.6, SD 25.3 percent of baseline) than during the Baseline (Tukey's HSD, $p<0.05$) and during Washout (109.8, SD 24.1 percent of baseline; Tukey's HSD $p<0.005$). Washout was not significantly different than the Baseline (Tukey's HSD, $p>0.05$). Therefore, bath-applied exogenous 5HT reduced NMDA-driven fictive motor bursting without significantly affecting the grouping of the bursts into swimming episodes.

The degree to which the ISNs are involved serotonergic modulation of locomotor output has not been demonstrated in zebrafish. The proximity of ISN projections to motor neurons led to the hypothesis that 5HT specifically derived from the ISNs modulates the spinal locomotor network (Van Raamsdonk et al., 1996; Brustein et al., 2003; McLean and Fetcho, 2004b). To test this hypothesis, we spinally transected 5–7 dpf larvae to remove the influence of the descending serotonergic raphe fibers. Baseline fictive locomotor activity was recorded in NMDA and an SSRI (citalopram hydrobromide) was bath-applied to inhibit reuptake of 5HT (Fig. 7) and thereby increase the amount of extracellular 5HT originating from the ISNs in the absence of intact raphe fibers. Treatment condition produced an effect on the total number of bursts recorded (single factor ANOVA, $F=9.95$, $p<0.005$; Fig. 7C), which was significantly lower than the Baseline during SSRI treatment (67.2, SD 11.3 percent of baseline; Tukey's HSD, $p<0.005$). Burst number was higher after Washout (87.9, SD 19.2 percent of baseline) than during SSRI treatment (Tukey's HSD, $p>0.05$) and was not significantly different from the Baseline (Tukey's HSD, $p>0.05$).

There was also a significant effect of SSRI treatment condition on the grouping of bursts into episodes (single factor ANOVA, $F=8.52$, $p<0.005$; Fig. 7D). EO score was significantly lower than the Baseline during SSRI treatment (77.6, SD 15.7 percent of baseline; Tukey's HSD, $p<0.05$) and Washout (75.2, SD 12.2 percent of baseline; Tukey's HSD, $p<0.01$). There was no significant difference in EO score between the SSRI treatment and Washout conditions (Tukey's HSD, $p<0.05$). Therefore, the SSRI reduced motor nerve bursting and episodic organization, and bursting returned to baseline levels after the Washout while the episodic organization of bursting did not.

Next, to directly test the effect of ISN activity on spinal locomotor network output, ChR2 was used to selectively activate the ISNs in transected SCs (Fig. 8). *Tg(pet1:gal4-p2A-EGFP)*^{gy1} crosses *Tg(UAS:ChR2(H134R)-mCherry)* produced specific expression of *ChR2-mCherry* in the ISNs. NMDA-induced fictive locomotor bursting activity was continuously recorded prior to (Baseline), during (Light), and following (Post) blue light illumination (Fig. 8A and B). Preparations were also illuminated with red light to verify that wavelengths of light outside of the range used to activate ChR2 did not affect locomotor activity (Supporting information, Fig. S1). There was a significant interaction between time (Baseline, Light, and Post light) and color of light (blue or red; two-factor ANOVA, $F=8.34$, $p<0.005$). Post-hoc testing revealed a significant reduction in bursting during blue light illumination (59.9, SD 31.3 percent of baseline; Tukey's HSD, $p<0.001$), which was also significantly lower than during post-blue light illumination (112.4, SD 19.2 percent of baseline; Tukey's HSD, $p<0.001$; Fig. 8C). We did not find a difference in burst number between the Baseline and Post light conditions (Tukey's HSD, $p>0.05$). Thus, activation of ISNs reduced the motor bursting output of the spinal locomotor network.

Although bursting was reduced in all of the preparations tested, the degree to which bursting was diminished was variable between preparations (Fig. 8B and C). Expression of *ChR2-mCherry* in double transgenic *Tg(pet1:gal4-p2A-EGFP)*^{gy1};*Tg(UAS:ChR2(H134R)-mCherry)* larvae was variegated (41.7%, SD 10.2 of EGFP-positive ISNs exhibited mCherry fluorescence), which is consistent with transgenerational silencing of *UAS*-driven transgenes (Goll et al., 2009; Akitake et al., 2011). A higher number of cells exhibiting mCherry fluorescence correlated with a greater reduction in bursting during blue light exposure compared to the Baseline (Fig. 8D). Therefore, individual differences may be due, in part, to the penetrance of *UAS:ChR2-mCherry* transgene expression. Altogether, these data suggest that 5HT released from the ISNs reduces spinally-generated locomotor activity.

Discussion

ISN number and location vary between vertebrate species. In fish, ISN cell somas and projections are commonly located near locomotor-generating regions of the SC (Parent and Northcutt, 1982; Harris-Warrick et al., 1985; Van Dongen et al., 1985a; Van Raamsdonk et al., 1996; Brustein et al., 2003; McLean and Fetcho, 2004a; McLean and Fetcho, 2004b) and spinally-endogenous 5HT modulates locomotor output in lamprey (Christenson et al., 1989; Zhang and Grillner, 2000; Wang et al., 2014). Although the zebrafish provides many added genetic and optical tools for investigating the relationship of the serotonergic system and locomotor network, a clear role for ISNs in modulating the spinal locomotor network has not

yet been demonstrated. The aim of this study was to build upon previous characterizations of zebrafish ISNs by incorporating newer labeling and optogenetic approaches to more clearly elucidate the development, morphology, and function of these cells.

Cell Number and Distribution

The *pet1* and *tph2*-expressing population of ISNs differentiates in the zebrafish SC between approximately 2.5 and 3 dpf, coinciding with the gradual loss of 5HT immunoreactivity in Kolmer-Agduhr neurons (Montgomery et al., 2016). The *Tg(pet1:EGFP)*^{ne0214} line permitted *in vivo* quantification of the number and distribution of later-developing ISNs at 3 dpf and onward (Fig. 1). ISN cell counts throughout the rostrocaudal extent of the SC (excluding the first two body segments) did not reveal a significant change in ISN cell number between 3 and 10 dpf, which was consistent with our quantifications in different SC regions (Montgomery et al., 2016). Cells were distributed evenly along the rostrocaudal axis with the exception of the caudal-most SC, in which a larger number of ISNs was observed (Fig. 1C and E) in 5, 7, and 10 dpf larvae, but not in 3 dpf larvae (not shown). This difference may have been due to the timing of development of these cells along the rostrocaudal axis (Montgomery et al., 2016), even though overall differences in cell number between these ages were not significant.

While ISNs were distributed along the entire rostrocaudal axis of the SC, irregular spacing between somas in individual larvae (Fig. 1A–C) indicated that ISNs were not segmentally distributed like the axial motor neurons (Myers, 1985). The position of ISNs within the larval SC was largely as expected (Brustein et al., 2003; McLean and Fetcho, 2004a) with somas arranged bilaterally along the SC floor, although we identified a relatively small number of somas that were more laterally located and/or did not contact the SC floor (Fig. 1D and G). Finally, the *pet1:EGFP* transgene continued to label ISNs in the adult SC (Fig. 1H and I). This, combined with the persistence of their ventral location, provides evidence that the identity of 5HT-ir cells does not undergo a major transition between larval and adult stages as it does between embryonic and larval stages of development (Montgomery et al., 2016).

Projection extension

ISNs are considered unipolar, with a single trunk extending from the soma and bifurcating into rostral dendritic projections and a single caudal axonal projection (Brustein et al., 2003; McLean and Fetcho, 2004a). Although mature serotonergic spinal innervation is achieved by 4 dpf (McLean and Fetcho, 2004a), the morphological development of individual ISNs has not yet been described. Therefore, we optically-isolated individual ISNs by photoconverting Kaede fluorescent protein in ISN somas to reveal morphology and to track projection growth over time. There was no significant change in rostral projection distance or neurite length at any of the ages studied (Fig. 3C; Table 1). This was likely due to high variability from 3 to 4 dpf; cells that had only begun to extend rostral projections when 3 dpf images were collected produced a much larger percent change than cells in which rostral projections had already formed. Sholl analysis indicated that the region with the greatest arborization corresponded to the rostral dendritic branches (Fig. 4B) and that the greatest number of intersections (critical value) increased significantly between 3 and 4 dpf (Fig. 3C; Table 1). Together, this

demonstrated that the dendrites underwent a large amount of change from 3 to 4 dpf, but that the amount of change was highly variable. Caudal projection distance and neurite length increased significantly from 3 to 4 and 4 to 5 dpf (Fig. 3C; Table 1). Thus, rostral projections achieved a stable innervation pattern by 4 dpf, while the caudal axonal projections did not until 5 dpf.

ISN axons terminated with enlarged structures (Fig. 4A) that have been described as growth cones (McLean and Fetcho, 2004a). Interestingly, these enlargements persisted at the terminals of fully-extended axons (Fig. 3A). We found that synaptic vesicles were localized to these structures at 5 dpf (Fig. 5). This indicated that ISN growth cones mature into functional synaptic terminals during, or shortly following axon extension. The large size of the terminals suggests that they may be specialized, potentially for volume transmission of 5HT. In agreement with this hypothesis, extrasynaptic volume transmission is considered to be the primary method of 5HT signaling in the lamprey SC (Christenson et al., 1990). The developmental transition and function of these terminals provides an intriguing direction for future work.

The overlap of serotonergic fibers labeled by 5HT antibodies and the *pet1:EGFP* transgene (Fig. 1A and B) led to uncertainty about the projection patterns and distances of ISNs (McLean and Fetcho, 2004a). Since ISN projections were collectively established by 5 dpf, we studied the morphometry of optically-isolated ISNs between 5 and 7 dpf. Surprisingly, a subset of ISNs appeared bipolar (16 out of 46), even though they possessed projection patterns that were similar to unipolar ISNs (Fig. 1A and B; Fig. 4A). Dorsal and lateral projection distances were short with little variability, while rostrocaudal projection distances and lengths were greater and relatively more variable (Fig. 4C). Identification of ISN projection targets may explain the variability that we observed in neurite lengths and projection distances (Fig. 4). Neurites projected laterally to the SC boundary as was previously described (Brustein et al., 2003; McLean and Fetcho, 2004a), although we identified a single contralateral projection (Fig. 4A, top row) in 3 of the 46 cells examined. Despite these differences between ISNs, we did not find morphological evidence of functionally-diverse populations of ISNs, since innervation patterns were wholly stereotypical.

Function of ISNs and spinally-intrinsic 5HT signaling

The proposed functional roles of ISNs vary between species and are commonly based upon ISN soma position and the regions of the SC that they innervate. ISNs in the mouse and rat are located dorsal to the central canal, are concentrated in certain rostrocaudal regions, and are hypothesized to modulate autonomic functions (Newton and Hamill, 1988). Chick and monkey ISNs project to the central canal, potentially regulating flow of cerebrospinal fluid or releasing 5HT into the central canal (Lamotte et al., 1982; Sako et al., 1986). These functions may be shared by the transiently 5HT-ir Kolmer-Agduhr neurons that contact the central canal in the embryonic zebrafish SC (Montgomery et al., 2016; Djenoune et al., 2017). ISNs are distributed evenly along the rostrocaudal axis in lamprey and zebrafish, near the locomotor circuitry in the ventral SC (Harris-Warrick et al., 1985; Van Dongen et al., 1985a; Van Raamsdonk et al., 1996; McLean and Fetcho, 2004b); Fig. 1).

Modulation of the spinal locomotor network by spinally-produced 5HT is well-established in lamprey (Christenson et al., 1989; Matsushima and Grillner, 1992; Zhang and Grillner, 2000; Schwartz et al., 2005), but has not been studied as extensively in zebrafish. Similar to lamprey (Harris-Warrick and Cohen, 1985; Christenson et al., 1989; Wallén et al., 1989), NMDA-induced fictive episode frequency is reduced when exogenous 5HT is applied to *in vitro* adult zebrafish hindbrain/SC preparations (Gabriel et al., 2009). Episode frequency is also reduced with application of the SSRI citalopram to adult hindbrain/SC preparations, providing evidence that 5HT released from the hindbrain and ISNs into the SC potentiates inhibition of locomotor activity (Gabriel et al., 2009).

Here, we tested the effect of spinal 5HT in spinally transected larvae. This contrasts with the study by Gabriel et al. (2009) in that we removed the hindbrain, leaving only the ISNs as a source of spinally-endogenous 5HT. We first tested the effects of bath-applied 5HT on locomotor activity (Fig. 6), which does not model physiological 5HT signaling since it is applied systemically to the entire SC. Next, we used citalopram to block reuptake of extracellular 5HT and test the effect of increased spinally-endogenous 5HT originating from the ISNs on locomotor output (Fig. 7). Finally, ChR2-mediated activation of the ISNs was used to test their role in modulating locomotor activity (Fig. 8). Each of these treatments led to a decrease in motor bursting, which was reversed when the experimental treatment was removed. This suggests that overall, both exogenous 5HT and endogenous 5HT released from the ISNs have an inhibitory effect on spinally-generated locomotor activity, in agreement with the reduced episode frequency observed in adult hindbrain/SC preparations (Gabriel et al., 2009). In our experimental paradigm, supraspinal sources of 5HT were removed by spinal transection; however, the raphe axons remained in the SC. Our conclusions are based on the assumption that 5HT was no longer released from the severed raphe fibers after removal of their dendrites, soma, and axon hillock. Peripheral nerve recordings were initiated a minimum of 30 min following spinal transection, although it is not known if the remaining severed fibers were still capable of 5HT release. Future work could either independently ablate these axons, or in some way confirm their loss of function.

In contrast to our larval spinal transection data, 5HT and 5HT-receptor agonists increase the frequency of swimming episodes in intact larvae (Brustein et al., 2003). The properties of the episodes themselves are not changed (Brustein et al., 2003), indicative of an overall increase in locomotor activity. This differed from the reduction in activity caused by 5HT and citalopram in the adult hindbrain/SC preps, hence Gabriel et al. (2009) proposed that this is due to the developmental stage of the animals. Since our findings in spinally-transected larvae more closely reflected the adult data, we suggest that the discrepancies are more likely due to the presence or absence of higher-order brain regions.

None of the previous zebrafish studies differentiated between spinal 5HT originating from the hindbrain and 5HT originating from the ISNs. We found that, after complete isolation of the SC from the brain, blocking 5HT reuptake and optogenetically activating the ISNs both caused an overall inhibition of motor nerve bursting (Fig. 7 and 8). This demonstrated that 5HT released from the ISNs is at least partially responsible for this effect. The effects of 5HT, citalopram, and ISN activation on the organization of bursts into swimming episodes were less clear. 5HT treatment did not produce a consistent effect on EO score (Fig. 6).

Citalopram did reduce EO score, but this effect did not wash out, even as the number of bursts did (Fig. 7). Finally, EO score could not be calculated during optogenetic ISN activation since some of the preparations showed such a dramatic reduction in burst number that there were too few bursts to analyze, although activity returned in all preparations following removal of the light stimulus (Fig. 8). This likely reflects that 5HT modulates locomotor at multiple levels in the spinal network, thus the targets of the ISNs and serotonergic raphe axons warrant investigation.

Conclusions

We incorporated a variety of optical imaging approaches to describe ISN distribution, morphology, and projection growth. ISN projections stabilized between 3 and 5 dpf, coinciding with the onset of mature swimming and hunting behavior (Budick and O'Malley, 2000; Buss and Drapeau, 2001). This is also the age at which treatment with compounds affecting serotonergic signaling are initially observed to produce an effect on locomotor output (Brustein et al., 2003; Brustein and Drapeau, 2005; Airhart et al., 2007). We presented evidence that the spinal locomotor network is modulated by spinally-intrinsic 5HT derived from the ISNs in zebrafish larvae. Developing a better understanding of the ISNs and their function in the larval zebrafish will provide a framework for comparative work with mammals, allowing evaluation of the effects of 5HT-rich and poor environments on spinal networks after transection of descending raphe processes.

Supplementary Material

Refer to Web version on PubMed Central for supplementary material.

Acknowledgments

The authors appreciate the helpful suggestions and feedback from Drs. Laure Bally-Cuif, Matthew Beckman, Aaron Lambert, Jack Peck, and Martin Wessendorf. We also thank Kayce Vanpelt for technical support and Marc Tye and the staff of the University of Minnesota Zebrafish Core Facility for animal care.

Financial Support: This work was supported by National Institutes of Health (http://www.nih.gov/) grants R01 NS065054 (MAM), R01 NS094176 (MAM), and F31 NS083110 (TDW). JM was supported by the University of Minnesota Bob Allison Ataxia Research Center (BAARC) and MnDRIVE Brain Conditions.

References

Airhart MJ, Lee DH, Wilson TD, Miller BE, Miller MN, Skalko RG. 2007; Movement disorders and neurochemical changes in zebrafish larvae after bath exposure to fluoxetine (PROZAC). Neurotoxicol Teratol. 29:652–664. [PubMed: 17761399]

Akitake CM, Macurak M, Halpern ME, Goll MG. 2011; Transgenerational analysis of transcriptional silencing in zebrafish. Dev Biol. 352:191–201. [PubMed: 21223961]

Andén NE, Häeggendal J, Magnusson T, Rosengren E. 1964; The Time Course of the Disappearance of Noradrenaline and 5-Hydroxytryptamine in the Spinal Cord after Transection. Acta Physiol Scand. 62:115–118. [PubMed: 14210252]

Ando R, Hama H, Yamamoto-Hino M, Mizuno H, Miyawaki A. 2002; An optical marker based on the UV-induced green-to-red photoconversion of a fluorescent protein. Proc Natl Acad Sci U S A. 99:12651–12656. [PubMed: 12271129]

Ballion B, Branchereau P, Chapron J, Viala D. 2002; Ontogeny of descending serotonergic innervation and evidence for intraspinal 5-HT neurons in the mouse spinal cord. Brain Res Dev Brain Res. 137:81–88. [PubMed: 12128257]

Barnes NM, Sharp T. 1999; A review of central 5-HT receptors and their function. Neuropharmacology. 38:1083–1152. [PubMed: 10462127]

Barreiro-Iglesias A, Mysiak KS, Scott AL, Reimer MM, Yang Y, Becker CG, Becker T. 2015; Serotonin Promotes Development and Regeneration of Spinal Motor Neurons in Zebrafish. Cell Rep. 13:924–932. [PubMed: 26565906]

Bellipanni G, Rink E, Bally-Cuif L. 2002; Cloning of two tryptophan hydroxylase genes expressed in the diencephalon of the developing zebrafish brain. Mech Dev. 119(Suppl 1):S215–220. [PubMed: 14516688]

Berger M, Gray JA, Roth BL. 2009; The expanded biology of serotonin. Annu Rev Med. 60:355–366. [PubMed: 19630576]

Billinton N, Knight AW. 2001; Seeing the wood through the trees: a review of techniques for distinguishing green fluorescent protein from endogenous autofluorescence. Anal Biochem. 291:175–197. [PubMed: 11401292]

Brustein E, Chong M, Holmqvist B, Drapeau P. 2003; Serotonin patterns locomotor network activity in the developing zebrafish by modulating quiescent periods. J Neurobiol. 57:303–322. [PubMed: 14608665]

Brustein E, Drapeau P. 2005; Serotoninergic modulation of chloride homeostasis during maturation of the locomotor network in zebrafish. J Neurosci. 25:10607–10616. [PubMed: 16291933]

Buckley K, Kelly RB. 1985; Identification of a transmembrane glycoprotein specific for secretory vesicles of neural and endocrine cells. J Cell Biol. 100:1284–1294. [PubMed: 2579958]

Budick SA, O'Malley DM. 2000; Locomotor repertoire of the larval zebrafish: swimming, turning and prey capture. J Exp Biol. 203:2565–2579. [PubMed: 10934000]

Bunin MA, Wightman RM. 1999; Paracrine neurotransmission in the CNS: involvement of 5-HT. Trends Neurosci. 22:377–382. [PubMed: 10441294]

Buss RR, Drapeau P. 2001; Synaptic drive to motoneurons during fictive swimming in the developing zebrafish. J Neurophysiol. 86:197–210. [PubMed: 11431502]

Carlsson A, Magnusson T, Rosengren E. 1963; 5-Hydroxytryptamine of the Spinal Cord Normally and after Transection. Experientia. 19:359.

Cazalets JR, Sqalli-Houssaini Y, Clarac F. 1992; Activation of the central pattern generators for locomotion by serotonin and excitatory amino acids in neonatal rat. J Physiol. 455:187–204. [PubMed: 1362441]

Christenson J, Cullheim S, Grillner S, Hökfelt T. 1990; 5-hydroxytryptamine immunoreactive varicosities in the lamprey spinal cord have no synaptic specializations--an ultrastructural study. Brain Res. 512:201–209. [PubMed: 2354357]

Christenson J, Franck J, Grillner S. 1989; Increase in endogenous 5-hydroxytryptamine levels modulates the central network underlying locomotion in the lamprey spinal cord. Neurosci Lett. 100:188–192. [PubMed: 2668801]

Clineschmidt BV, Pierce JE, Lovenberg W. 1971; Tryptophan hydroxylase and serotonin in spinal cord and brain stem before and after chronic transection. J Neurochem. 18:1593–1596. [PubMed: 5092876]

Dahlström A, Fuxe K. 1964; Localization of monoamines in the lower brain stem. Experientia. 20:398–399. [PubMed: 5856530]

Djenoune L, Desban L, Gomez J, Sternberg JR, Prendergast A, Langui D, Quan FB, Marnas H, Auer TO, Rio JP, Del Bene F, Bardet PL, Wyart C. 2017; The dual developmental origin of spinal cerebrospinal fluid-contacting neurons gives rise to distinct functional subtypes. Sci Rep. 7:719. [PubMed: 28389647]

Ferreira TA, Blackman AV, Oyrer J, Jayabal S, Chung AJ, Watt AJ, Sjöström PJ, van Meyel DJ. 2014; Neuronal morphometry directly from bitmap images. Nat Methods. 11:982–984. [PubMed: 25264773]

Fuxe K, Dahlström A, Höistad M, Marcellino D, Jansson A, Rivera A, Diaz-Cabiale Z, Jacobsen K, Tinner-Staines B, Hagman B, Leo G, Staines W, Guidolin D, Kehr J, Genedani S, Belluardo N,

Agnati LF. 2007; From the Golgi-Cajal mapping to the transmitter-based characterization of the neuronal networks leading to two modes of brain communication: wiring and volume transmission. Brain Res Rev. 55:17–54. [PubMed: 17433836]

Gabriel JP, Mahmood R, Kyriakatos A, Söll I, Hauptmann G, Calabrese RL, El Manira A. 2009; Serotonergic modulation of locomotion in zebrafish: endogenous release and synaptic mechanisms. J Neurosci. 29:10387–10395. [PubMed: 19692613]

Ghosh M, Pearse DD. 2014; The role of the serotonergic system in locomotor recovery after spinal cord injury. Front Neural Circuits. 8:151. [PubMed: 25709569]

Goll MG, Anderson R, Stainier DY, Spradling AC, Halpern ME. 2009; Transcriptional silencing and reactivation in transgenic zebrafish. Genetics. 182:747–755. [PubMed: 19433629]

Harris-Warrick RM, Cohen AH. 1985; Serotonin modulates the central pattern generator for locomotion in the isolated lamprey spinal cord. J Exp Biol. 116:27–46. [PubMed: 4056654]

Harris-Warrick RM, McPhee JC, Filler JA. 1985; Distribution of serotonergic neurons and processes in the lamprey spinal cord. Neuroscience. 14:1127–1140. [PubMed: 3889703]

Holst J, Vignali KM, Burton AR, Vignali DA. 2006; Rapid analysis of T-cell selection in vivo using T cell-receptor retrogenic mice. Nat Methods. 3:191–197. [PubMed: 16489336]

Hoyer D, Clarke DE, Fozard JR, Hartig PR, Martin GR, Mylecharane EJ, Saxena PR, Humphrey PP. 1994; International Union of Pharmacology classification of receptors for 5-hydroxytryptamine (Serotonin). Pharmacol Rev. 46:157–203. [PubMed: 7938165]

Kawakami K. 2004; Transgenesis and gene trap methods in zebrafish by using the Tol2 transposable element. Methods Cell Biol. 77:201–222. [PubMed: 15602913]

Köster RW, Fraser SE. 2001; Tracing transgene expression in living zebrafish embryos. Dev Biol. 233:329–346. [PubMed: 11336499]

Kuscha V, Barreiro-Iglesias A, Becker CG, Becker T. 2011Plasticity of tyrosine hydroxylase and serotonergic systems in the regenerating spinal cord of adult zebrafish. J Comp Neurol.

Kwan KM, Fujimoto E, Grabher C, Mangum BD, Hardy ME, Campbell DS, Parant JM, Yost HJ, Kanki JP, Chien CB. 2007; The Tol2kit: a multisite gateway-based construction kit for Tol2 transposon transgenesis constructs. Dev Dyn. 236:3088–3099. [PubMed: 17937395]

Lambert AM, Bonkowsky JL, Masino MA. 2012; The conserved dopaminergic diencephalospinal tract mediates vertebrate locomotor development in zebrafish larvae. J Neurosci. 32:13488–13500. [PubMed: 23015438]

Lamotte CC, Johns DR, de Lanerolle NC. 1982; Immunohistochemical evidence of indolamine neurons in monkey spinal cord. J Comp Neurol. 206:359–370. [PubMed: 7047583]

Lillesaar C. 2011; The serotonergic system in fish. J Chem Neuroanat. 41:294–308. [PubMed: 21635948]

Lillesaar C, Stigloher C, Tannhäuser B, Wullimann MF, Bally-Cuif L. 2009; Axonal projections originating from raphe serotonergic neurons in the developing and adult zebrafish, Danio rerio, using transgenics to visualize raphe-specific pet1 expression. J Comp Neurol. 512:158–182. [PubMed: 19003874]

Lillesaar C, Tannhäuser B, Stigloher C, Kremmer E, Bally-Cuif L. 2007; The serotonergic phenotype is acquired by converging genetic mechanisms within the zebrafish central nervous system. Dev Dyn. 236:1072–1084. [PubMed: 17304529]

Liu C, Maejima T, Wyler SC, Casadesus G, Herlitze S, Deneris ES. 2010; Pet-1 is required across different stages of life to regulate serotonergic function. Nat Neurosci. 13:1190–1198. [PubMed: 20818386]

Longair MH, Baker DA, Armstrong JD. 2011; Simple Neurite Tracer: open source software for reconstruction, visualization and analysis of neuronal processes. Bioinformatics. 27:2453–2454. [PubMed: 21727141]

Masino MA, Fetcho JR. 2005; Fictive swimming motor patterns in wild type and mutant larval zebrafish. J Neurophysiol. 93:3177–3188. [PubMed: 15673549]

Matsushima T, Grillner S. 1992; Local serotonergic modulation of calcium-dependent potassium channels controls intersegmental coordination in the lamprey spinal cord. J Neurophysiol. 67:1683–1690. [PubMed: 1629770]

McDearmid JR, Drapeau P. 2006; Rhythmic motor activity evoked by NMDA in the spinal zebrafish larva. J Neurophysiol. 95:401–417. [PubMed: 16207779]

McLean DL, Fetcho JR. 2004a; Ontogeny and innervation patterns of dopaminergic, noradrenergic, and serotonergic neurons in larval zebrafish. J Comp Neurol. 480:38–56. [PubMed: 15515022]

McLean DL, Fetcho JR. 2004b; Relationship of tyrosine hydroxylase and serotonin immunoreactivity to sensorimotor circuitry in larval zebrafish. J Comp Neurol. 480:57–71. [PubMed: 15514919]

Montgomery JE, Wiggin TD, Rivera-Perez LM, Lillesaar C, Masino MA. 2016; Intraspinal serotonergic neurons consist of two, temporally distinct populations in developing zebrafish. Dev Neurobiol. 76:673–687. [PubMed: 26437856]

Myers PZ. 1985; Spinal motoneurons of the larval zebrafish. J Comp Neurol. 236:555–561. [PubMed: 4056102]

Newton BW, Hamill RW. 1988; The morphology and distribution of rat serotoninergic intraspinal neurons: an immunohistochemical study. Brain Res Bull. 20:349–360. [PubMed: 3365563]

Newton BW, Maley BE, Hamill RW. 1986; Immunohistochemical demonstration of serotonin neurons in autonomic regions of the rat spinal cord. Brain Res. 376:155–163. [PubMed: 3719364]

Nishimaru H, Takizawa H, Kudo N. 2000; 5-Hydroxytryptamine-induced locomotor rhythm in the neonatal mouse spinal cord in vitro. Neurosci Lett. 280:187–190. [PubMed: 10675792]

Onstott D, Elde R. 1986; Immunohistochemical localization of urotensin I/corticotropin-releasing factor, urotensin II, and serotonin immunoreactivities in the caudal spinal cord of nonteleost fishes. J Comp Neurol. 249:205–225. [PubMed: 3525617]

Parent A, Northcutt RG. 1982; The monoamine-containing neurons in the brain of the garfish, Lepisosteus osseus. Brain Res Bull. 9:189–204. [PubMed: 6129036]

Preibisch S, Saalfeld S, Tomancak P. 2009; Globally optimal stitching of tiled 3D microscopic image acquisitions. Bioinformatics. 25:1463–1465. [PubMed: 19346324]

Ridet JL, Rajaofetra N, Teilhac JR, Geffard M, Privat A. 1993; Evidence for nonsynaptic serotonergic and noradrenergic innervation of the rat dorsal horn and possible involvement of neuron-glia interactions. Neuroscience. 52:143–157. [PubMed: 8381923]

Ritchie TC, Leonard RB. 1982; Immunocytochemical demonstration of serotonergic cells, terminals and axons in the spinal cord of the stingray, Dasyatis sabina. Brain Res. 240:334–337. [PubMed: 7049319]

Rossignol S, Dubuc R. 1994; Spinal pattern generation. Curr Opin Neurobiol. 4:894–902. [PubMed: 7888774]

Sako H, Kojima T, Okado N. 1986; Immunohistochemical study on the development of serotoninergic neurons in the chick: II. Distribution of cell bodies and fibers in the spinal cord. J Comp Neurol. 253:79–91. [PubMed: 3540037]

Schindelin J, Arganda-Carreras I, Frise E, Kaynig V, Longair M, Pietzsch T, Preibisch S, Rueden C, Saalfeld S, Schmid B, Tinevez JY, White DJ, Hartenstein V, Eliceiri K, Tomancak P, Cardona A. 2012; Fiji: an open-source platform for biological-image analysis. Nat Methods. 9:676–682. [PubMed: 22743772]

Schmidt BJ, Jordan LM. 2000; The role of serotonin in reflex modulation and locomotor rhythm production in the mammalian spinal cord. Brain Res Bull. 53:689–710. [PubMed: 11165804]

Schnell SA, Staines WA, Wessendorf MW. 1999; Reduction of lipofuscin-like autofluorescence in fluorescently labeled tissue. J Histochem Cytochem. 47:719–730. [PubMed: 10330448]

Schwartz EJ, Gerachshenko T, Alford S. 2005; 5-HT prolongs ventral root bursting via presynaptic inhibition of synaptic activity during fictive locomotion in lamprey. J Neurophysiol. 93:980–988. [PubMed: 15456802]

Scott EK, Mason L, Arrenberg AB, Ziv L, Gosse NJ, Xiao T, Chi NC, Asakawa K, Kawakami K, Baier H. 2007; Targeting neural circuitry in zebrafish using GAL4 enhancer trapping. Nat Methods. 4:323–326. [PubMed: 17369834]

Shibuya T, Anderson EG. 1968; The influence of chronic cord transection on the effects of 5-hydroxytryptophan, l-tryptophan and pargyline on spinal neuronal activity. J Pharmacol Exp Ther. 164:185–190. [PubMed: 5303400]

Sillar KT, Reith CA, McDearmid JR. 1998; Development and aminergic neuromodulation of a spinal locomotor network controlling swimming in Xenopus larvae. Ann N Y Acad Sci. 860:318–332. [PubMed: 9928322]

Steinbusch HW. 1981; Distribution of serotonin-immunoreactivity in the central nervous system of the rat-cell bodies and terminals. Neuroscience. 6:557–618. [PubMed: 7017455]

Steinbusch HW, Verhofstad AA, Joosten HW. 1978; Localization of serotonin in the central nervous system by immunohistochemistry: description of a specific and sensitive technique and some applications. Neuroscience. 3:811–819. [PubMed: 362232]

Steinkamp JA, Stewart CC. 1986; Dual-laser, differential fluorescence correction method for reducing cellular background autofluorescence. Cytometry. 7:566–574. [PubMed: 3780360]

Tye M, Rider D, Duffy EA, Seubert A, Lothert B, Schimmenti LA. 2015; Nonhatching Decapsulated Artemia Cysts As a Replacement to Artemia Nauplii in Juvenile and Adult Zebrafish Culture. Zebrafish. 12:457–461. [PubMed: 25495227]

Van Dongen PA, Hökfelt T, Grillner S, Verhofstad AA, Steinbusch HW. 1985a; Possible target neurons of 5-hydroxytryptamine fibers in the lamprey spinal cord: immunohistochemistry combined with intracellular staining with Lucifer yellow. J Comp Neurol. 234:523–535. [PubMed: 3886717]

Van Dongen PA, Hökfelt T, Grillner S, Verhofstad AA, Steinbusch HW, Cuello AC, Terenius L. 1985b; Immunohistochemical demonstration of some putative neurotransmitters in the lamprey spinal cord and spinal ganglia: 5-hydroxytryptamine-, tachykinin-, and neuropeptide-Y-immunoreactive neurons and fibers. J Comp Neurol. 234:501–522. [PubMed: 2859306]

Van Raamsdonk W, Bosch TJ, Smit-Onel MJ, Maslam S. 1996; Organisation of the zebrafish spinal cord: distribution of motoneuron dendrites and 5-HT containing cells. Eur J Morphol. 34:65–77. [PubMed: 9090993]

Viala D, Buser P. 1974; Effects of a decarboxylase inhibitor on the Dopa and 5-HTP induced changes in the locomotor-like discharge pattern of rabbit hind limb nerves. Psychopharmacologia. 40:225–233. [PubMed: 4548539]

Wallace JA, Allgood PC, Hoffman TJ, Mondragon RM, Maez RR. 1986; Analysis of the change in number of serotonergic neurons in the chick spinal cord during embryonic development. Brain Res Bull. 17:297–305. [PubMed: 3533221]

Wallén P, Buchanan JT, Grillner S, Hill RH, Christenson J, Hökfelt T. 1989; Effects of 5-hydroxytryptamine on the afterhyperpolarization, spike frequency regulation, and oscillatory membrane properties in lamprey spinal cord neurons. J Neurophysiol. 61:759–768. [PubMed: 2542472]

Wang D, Grillner S, Wallén P. 2014; Endogenous release of 5-HT modulates the plateau phase of NMDA-induced membrane potential oscillations in lamprey spinal neurons. J Neurophysiol. 112:30–38. [PubMed: 24740857]

Wiggin TD, Anderson TM, Eian J, Peck JH, Masino MA. 2012; Episodic swimming in the larval zebrafish is generated by a spatially distributed spinal network with modular functional organization. Journal of Neurophysiology. 108:925–934. [PubMed: 22572943]

Xing L, Son JH, Stevenson TJ, Lillesaar C, Bally-Cuif L, Dahl T, Bonkowsky JL. 2015; A Serotonin Circuit Acts as an Environmental Sensor to Mediate Midline Axon Crossing through EphrinB2. J Neurosci. 35:14794–14808. [PubMed: 26538650]

Yokogawa T, Hannan MC, Burgess HA. 2012; The dorsal raphe modulates sensory responsiveness during arousal in zebrafish. J Neurosci. 32:15205–15215. [PubMed: 23100441]

Zhang F, Wang LP, Brauner M, Liewald JF, Kay K, Watzke N, Wood PG, Bamberg E, Nagel G, Gottschalk A, Deisseroth K. 2007; Multimodal fast optical interrogation of neural circuitry. Nature. 446:633–639. [PubMed: 17410168]

Zhang W, Grillner S. 2000; The spinal 5-HT system contributes to the generation of fictive locomotion in lamprey. Brain Res. 879:188–192. [PubMed: 11011021]

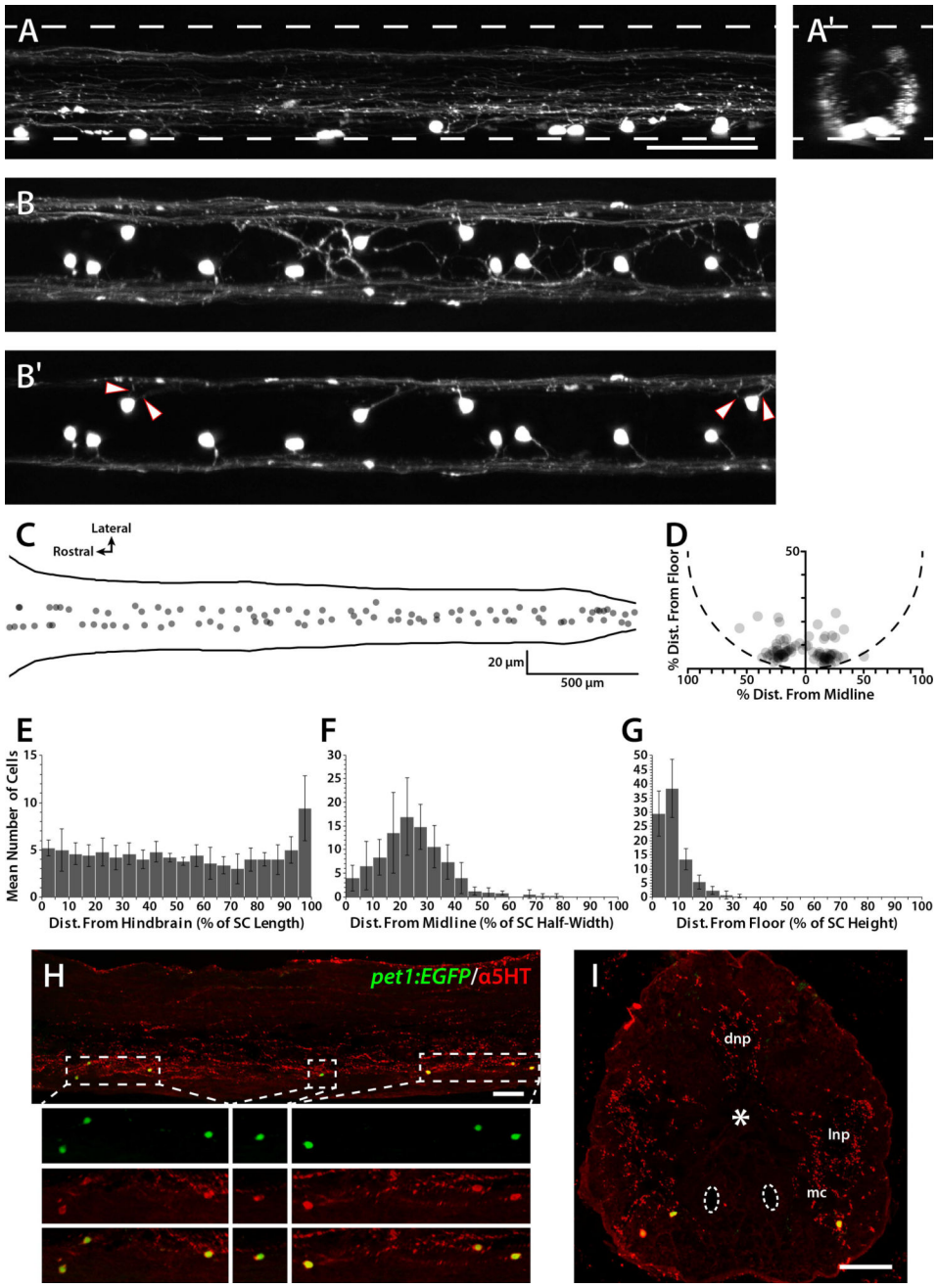

Figure 1. Location and distribution of *pet1:EGFP*-expressing ISNs

Confocal Z-stacks were collected from live 5 dpf *Tg(pet1:EGFP)*^{ne0214} SCs (A and B) and EGFP-labeled soma positions were plotted along the rostrocaudal, mediolateral, and dorsoventral axes (C and D). A and A′: A confocal Z-stack was collected from the lateral perspective of the midbody region (A) and rotated 90 degrees along the dorsoventral axis to create a transverse perspective (A′). Upper and lower dashed lines represent the dorsal and ventral boundaries of the SC, respectively. B and B′: A confocal Z-stack was collected from the dorsal perspective of the midbody region and projected to include the entire dorsoventral extent of the SC (B) and to include approximately only the ventral-most one-third of the SC,

highlighting projections from the ISN somas (B′). Arrowheads indicate lateral projections from somas from which two projections originated. C and D: The positions of all ISN somas in a single SC were plotted according to rostrocaudal and mediolateral position (C, solid lines represent the lateral edges of the SC), and dorsoventral and mediolateral position (D, dashed semicircle approximates the ventral SC boundary; soma position is normalized to account for differences in SC height and width along the rostrocaudal axis). E-G: ISN soma positions from 5 larvae were divided into 20 bins based on rostrocaudal distance from the hindbrain/SC boundary (E), lateral distance from the midline (F), and distance from the SC floor (G). H and I: Adult *Tg(pet1:EGFP)*^{ne0214} SC sections were labeled with antibodies to 5HT (red). Dashed boxes in sagittal sections (H) indicate regions in which Z-projections were restricted to cell somas and enlarged 2× in the subpanels below. Antibodies detected fibers throughout the dorsal neuropil (dnp), lateral neuropil (lnp), and in the motor column (mc; asterisk and dashed ovals represent the central canal and mauthner axons, respectively) in transverse sections (I). Antibody labeling of cell somas was restricted to those that expressed the *pet1:EGFP* transgene (green), which were located in, or near, the motor column in the ventral SC. Scale bars = 50 μm (scale bar in A applies to A–B′). Error bars represent SD.

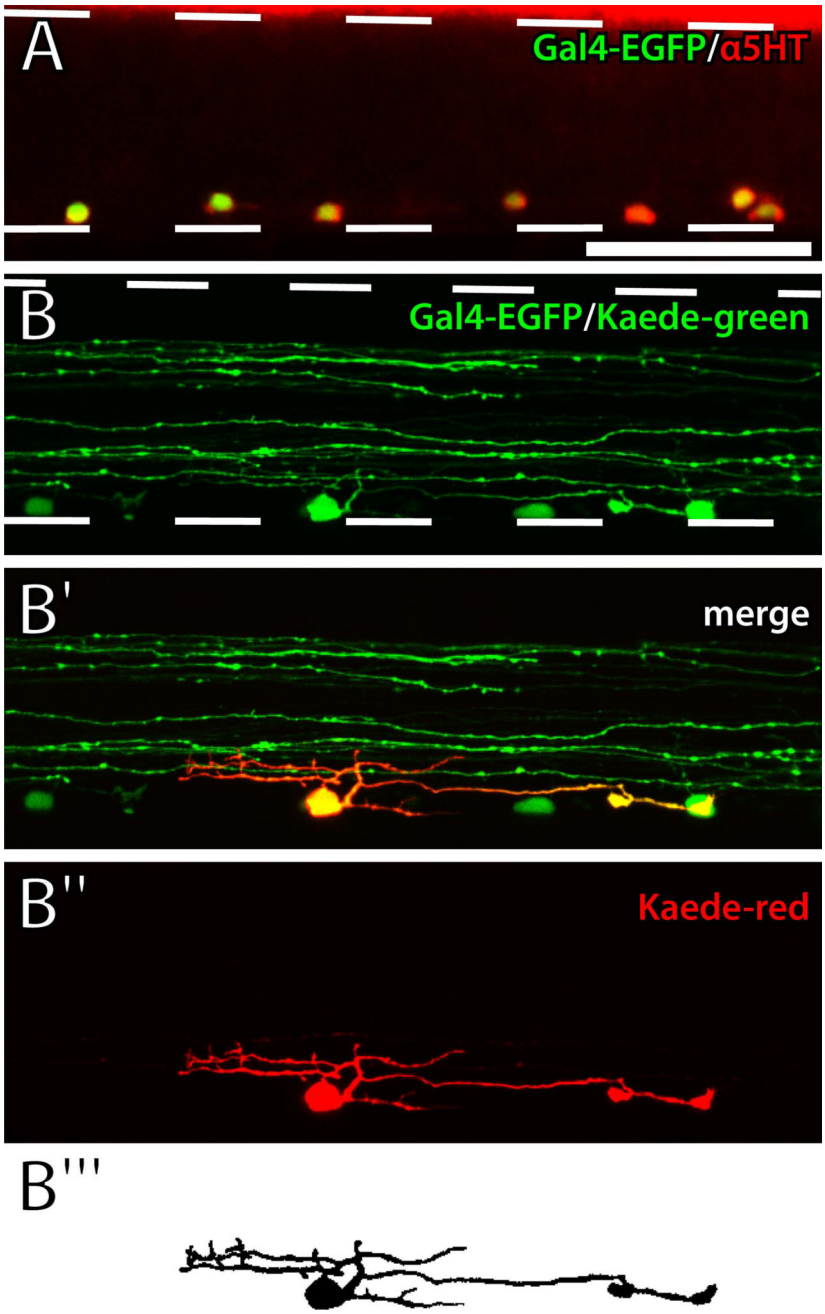

Figure 2. Optical isolation of ISNs

A: *Gal4-p2A-EGFP* transgene expression (green) overlapped with 5HT antibody labeling (red) in a 5 dpf *Tg(pet1:Gal4-p2A-EGFP)*^{gy1} larval SC. B: UV light was applied to a single ISN soma in a live *Tg(pet1:Gal4-p2A-EGFP)*^{gy1};*Tg(UAS:Kaede)*^{s1999t} larva. EGFP and green Kaede were expressed in ventrally-located ISN somas and nerve fibers in the dorsal and ventral SC (B; dashed lines represent the dorsal and ventral boundaries of the SC). Red Kaede fluorescence revealed a single ISN (red) that was optically isolated from other ISNs and descending nerve fibers (green; B′ and B″). Photoconverted red Kaede fluorescence

was used to create a thresholded representation of the ISN (B‴). Scale bar = 50 μm (applies to all panels).

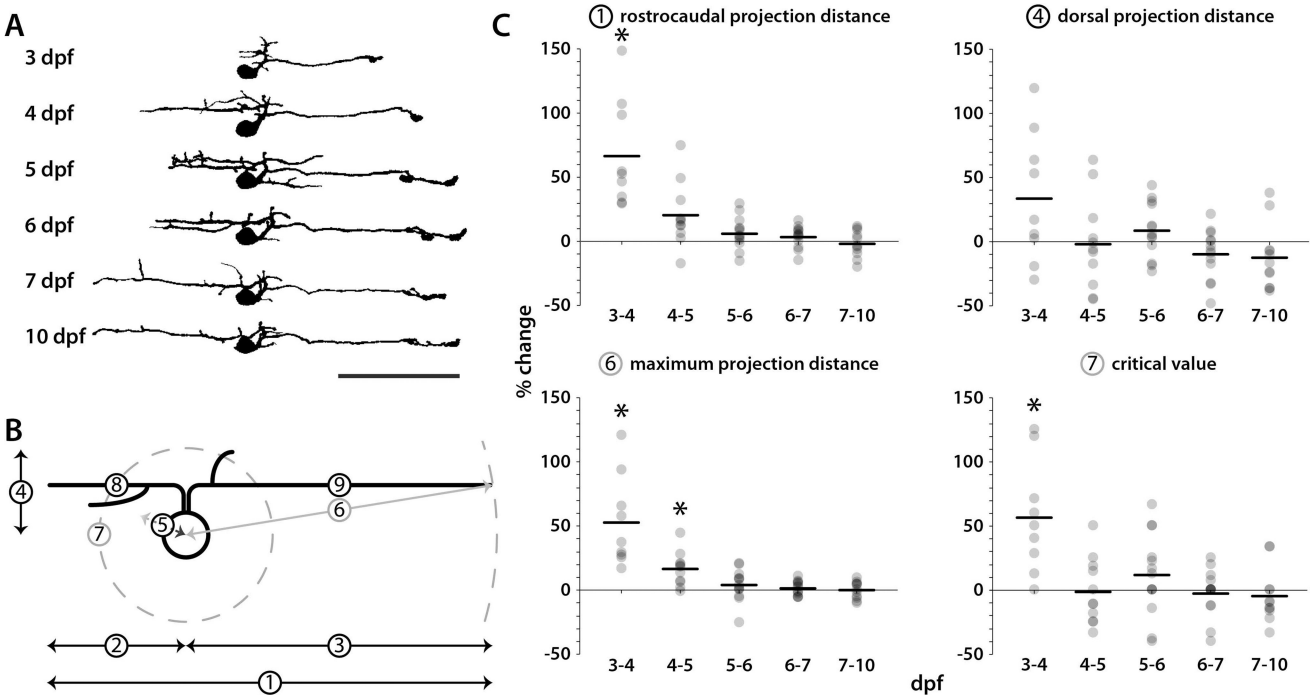

Figure 3. Changes in ISN morphology during larval development

Kaede was photoconverted in individual ISNs at 3, 4, or 5 dpf and confocal stacks of red Kaede fluorescence were collected and analyzed from the same cell at later timepoints up to 10 dpf. A: Traced and thresholded images of a single photoconverted ISN were collected at 3–7 and 10 dpf (rostral is left, dorsal is up). B: Morphometric properties of each ISN were measured at each timepoint: rostrocaudal projection distance (1), rostral projection distance (2), caudal projection distance (3), dorsal projection distance (4), lateral projection distance (5), maximum projection distance (6), critical value (7), rostral neurite length (8), and caudal neurite length (9). C: The percent change in rostrocaudal projection distance, dorsal projection distance, maximum projection distance, and critical value from one day to the next were plotted for each ISN (gray dots; horizontal bars indicate means; asterisks indicate a percent change significantly different from zero). Statistically significant changes to morphological features were not observed after 5 dpf. Scale bar = 50 μm (applies to A).

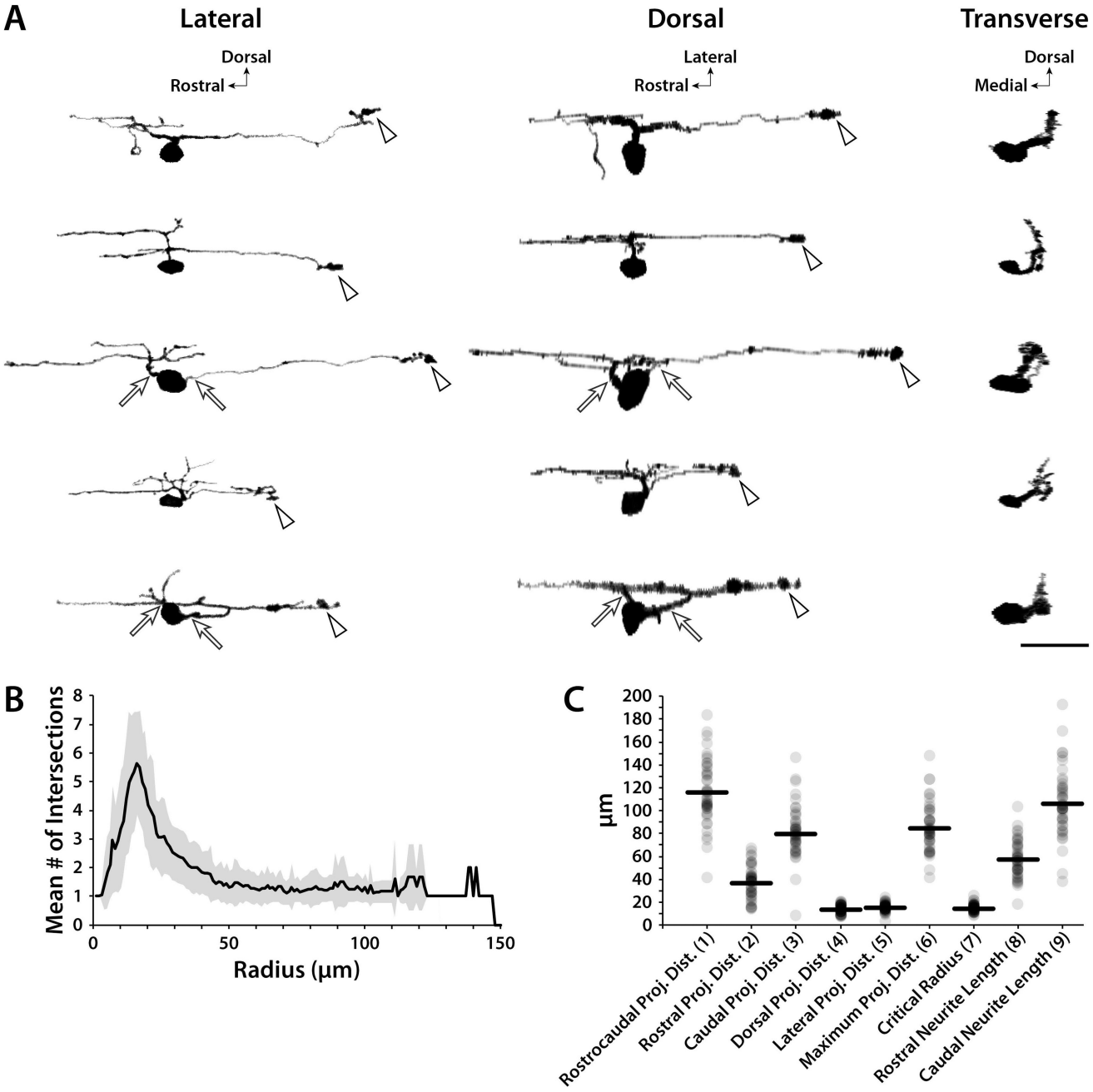

Figure 4. Morphological characteristics of ISNs

Kaede was photoconverted in individual 5–7 dpf ISNs and morphometry was quantified in confocal Z-stacks. A: Lateral confocal images of representative ISNs were rotated along the X and Y axes to simulate dorsal and transverse perspectives, respectively. The majority of ISNs extended one projection from the soma (30 of 46), while the others (16 of 46) extended two (arrows). Arrowheads indicate enlarged structures at axon terminals. B: Three-dimensional Sholl data was plotted as the mean number of intersections at radii originating from the center of the soma (gray area represents SD). The largest mean number of intersections occurred at a radius of 16 μm. C: Neurite projection distances, lengths, and

critical radii were plotted for each ISN (gray dots; black horizontal lines indicate means). Parenthetical numbers in X-axis labels correspond to the diagram in Fig. 3B. Scale bar = 25 μm (applies to A).

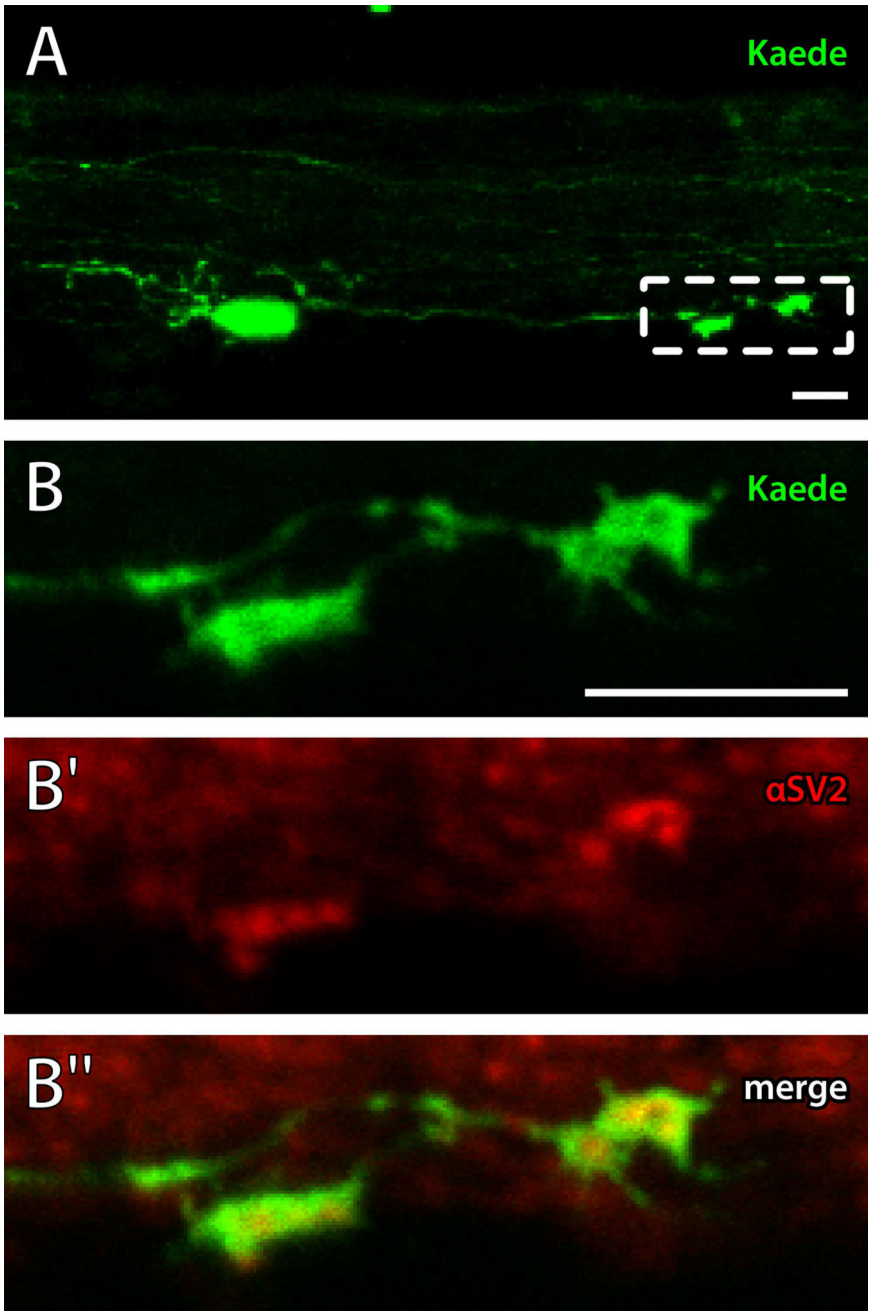

Figure 5. Caudal ISN projection terminals contain synaptic vesicles

Kaede was photoconverted in the ISNs (pseudocolored green) and 5 dpf larvae were labeled with antibodies to SV2 (pseudocolored red) to mark synaptic vesicles. A: A confocal Z-projection of a single ISN and its rostral and caudal processes. Dashed box indicates region shown in B. B-B″: A single-plane confocal image was collected of the caudal projection terminal showing overlap of Kaede (green; B and B″) and punctate SV2 antibody labeling (red; B′ and B″) at the terminals. Left is rostral, up is dorsal. Scale bars = 10 μm.

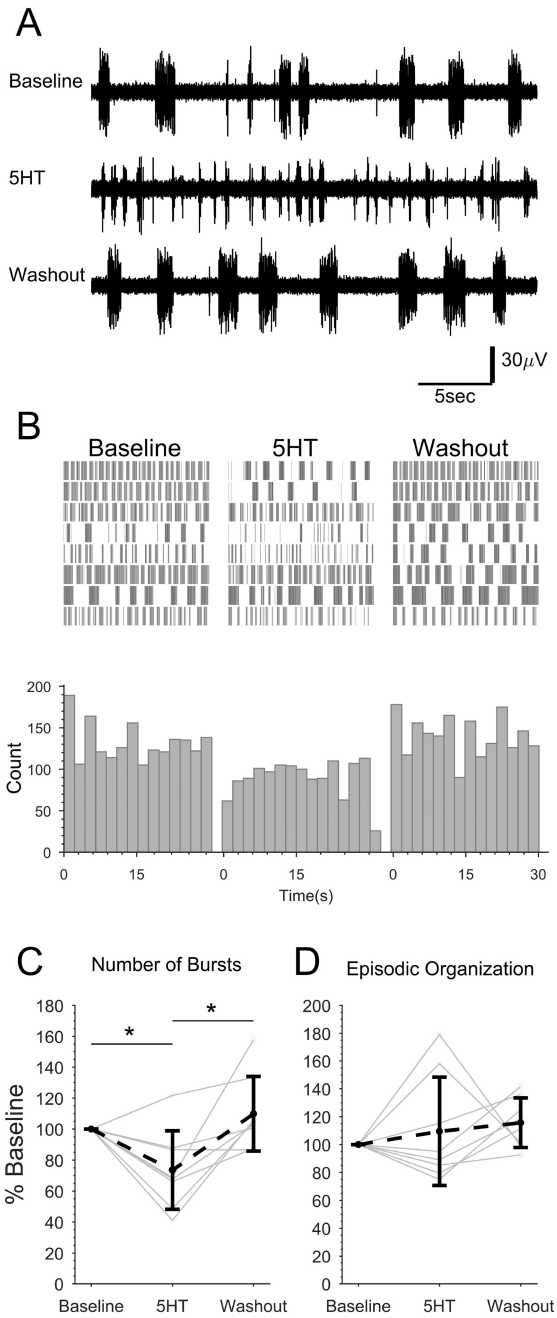

Figure 6. Exogenous 5HT reduces NMDA-induced fictive locomotor bursting in spinally-transected larvae

Spinally-transected larvae were continuously perfused with NMDA to induce fictive swimming activity. The final 2 min of 30 min Baseline, 15 min 5HT (1 μM) treatment, and 30 min Washout recordings were analyzed from each preparation. A: Representative peripheral motor nerve voltage traces from one preparation in each condition. B: Burst times were plotted (vertical lines) for each treatment condition. Each row represents one preparation (n=8). Bursts were binned and summated below. C and D: The total number of bursts (C) and the episodic organization of the bursts (D) under each condition were quantified and expressed as percent of baseline for each preparation (gray dots and lines)

and the mean of all preparations (black dots and dashed line). Asterisks indicate statistically significant differences. Error bars represent SD.

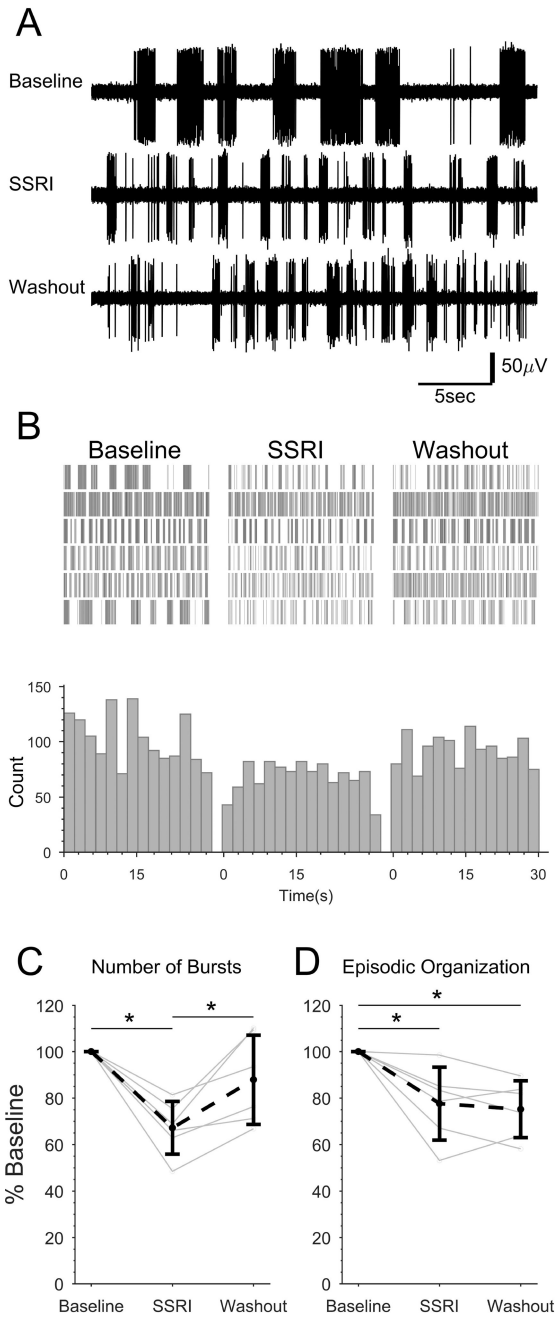

Figure 7. SSRI application reduces NMDA-induced fictive locomotor bursting and organization in spinally-transected larvae

Spinally-transected larvae were continuously perfused with NMDA to induce fictive swimming activity. The final 2 min of 30 min Baseline, 15 min SSRI (5 μM citalopram) treatment, and 30 min Washout recordings were analyzed from each preparation. A: Representative peripheral motor nerve voltage traces from one preparation in each condition. B: Burst times were plotted (vertical lines) for each treatment condition. Each row represents one preparation (n=6). Bursts were binned and summated below. C and D: The total number of bursts (C) and the episodic organization of the bursts (D) under each condition were quantified and expressed as percent of baseline for each preparation (gray dots and lines)

and the mean of all preparations (black dots and dashed line). Asterisks indicate statistically significant differences. Error bars represent SD.

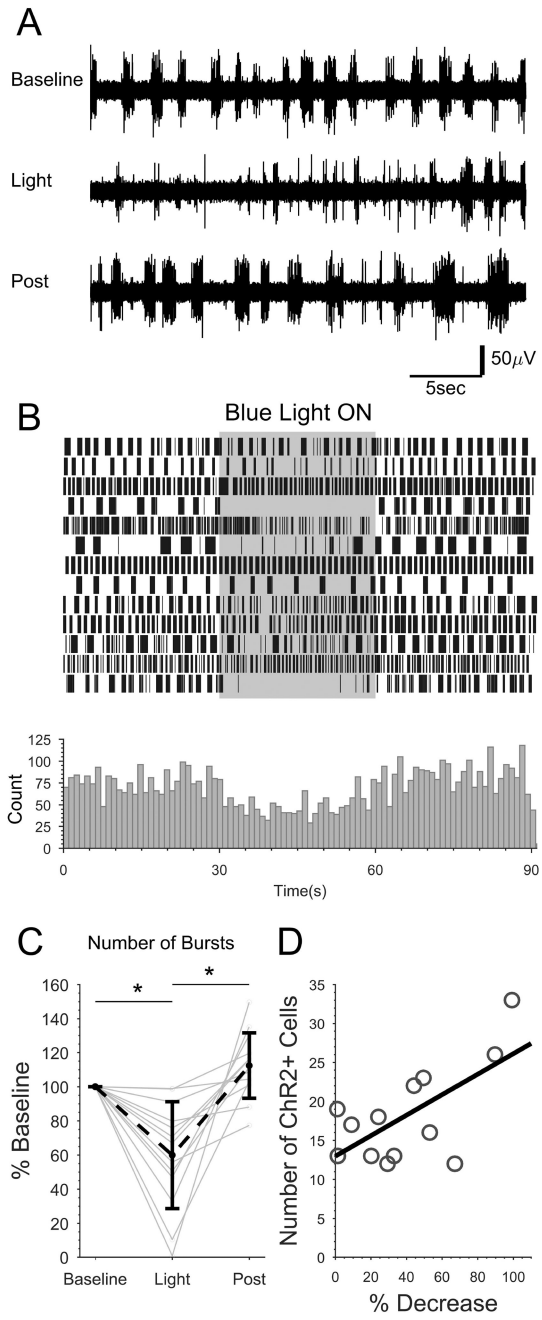

Figure 8. Optogenetic activation of ISNs reduces NMDA-induced fictive locomotor bursting in spinally-transected larvae

Spinally-transected *Tg(pet1:gal4-p2A-EGFP)*^{gy1};*Tg(UAS:ChR2(H134R)-mCherry)* larvae that expressed *ChR2-mCherry* in a subset of ISNs were perfused with NMDA to induce fictive swimming activity, then were exposed to a 30 s train of blue light pulses. A: Representative contiguous peripheral motor nerve voltage traces from one preparation before (Baseline), during (Light), and after (Post) blue light exposure. B: Continuous plot of burst times (vertical lines). Each row represents one preparation (n=13). Bursts were binned and summated below. C: The total number of bursts under each condition were quantified and expressed as percent of baseline for each preparation (gray dots and lines) and the mean of

all preparations (black dots and dashed line). Asterisks indicate statistically significant differences. Error bars represent SD. D: The number of *ChR2-mCherry* expressing cells was quantified in the skinned region of each preparation and plotted against the percent change in burst number. The number of *ChR2-mCherry* expressing cells positively correlated with a greater decrease in bursting activity when exposed to blue light (R^2=0.42).

Table 1

Morphometric changes to ISN projections in developing larvae

The percent change was calculated for each ISN from one age to the next and expressed as mean percent change ± SD. Parenthetical numbers in the measurement column correspond to the diagram in Fig. 3B.

	Percent change by larval age range (days post-fertilization)				
Measurement	**3–4 (n=9)**	**4–5 (n=11)**	**5–6 (n=13)**	**6–7 (n=13)**	**7–10 (n=11)**
Rostrocaudal Proj. Distance (1)	66.5 ± 41.5*	20.0 ± 24.5	6.1 ± 12.3	3.3 ± 8.4	−2.2 ± 10.4
Rostral Proj. Distance (2)	368.0 ± 496.6	44.8 ± 100.6	35.2 ± 81.3	7.4 ± 31.6	−1.0 ± 22.0
Caudal Proj. Distance (3)	41.7 ± 37.3*	16.6 ± 14.4*	6.4 ± 12.1	2.6 ± 7.7	−0.5 ± 8.6
Dorsal Proj. Distance (4)	33.1 ± 50.5	−2.0 ± 35.5	8.4 ± 21.4	−9.9 ± 19.4	−12.6 ± 25.5
Lateral Proj. Distance (5)	8.6 ± 23.8	6.9 ± 28.8	0.2 ± 22.8	6.2 ± 15.4	5.1 ± 11.9
Maximum Proj. Distance (6)	52.4 ± 35.2*	16.0 ± 12.9*	3.6 ± 12.1	1.3 ± 5.4	−0.3 ± 6.6
Critical Value (7)	56.4 ± 43.6*	−1.5 ± 25.6	11.6 ± 32.3	−2.7 ± 18.6	−4.8 ± 21.1
Rostral Neurite Length (8)	103.2 ± 110.8	18.1 ± 46.7	21.1 ± 42.4	−5.0 ± 20.5	−2.0 ± 16.2
Caudal Neurite Length (9)	44.1 ± 33.7*	15.5 ± 15.7*	9.6 ± 12.3	−1.1 ± 6.6	0.5 ± 5.6

Asterisks indicate a percent change that is significantly different than zero (corrected t-test, $p<0.05$).